



HAL
open science

Projected future changes in tropical cyclone-related wave climate in the North Atlantic

Ali Belmadani, Alice Dalphinnet, F. Chauvin, Romain Pilon, Philippe Palany

► **To cite this version:**

Ali Belmadani, Alice Dalphinnet, F. Chauvin, Romain Pilon, Philippe Palany. Projected future changes in tropical cyclone-related wave climate in the North Atlantic. *Climate Dynamics*, 2021, 10.1007/s00382-021-05664-5 . meteo-03134618

HAL Id: meteo-03134618

<https://meteofrance.hal.science/meteo-03134618v1>

Submitted on 9 Oct 2024

HAL is a multi-disciplinary open access archive for the deposit and dissemination of scientific research documents, whether they are published or not. The documents may come from teaching and research institutions in France or abroad, or from public or private research centers.

L'archive ouverte pluridisciplinaire **HAL**, est destinée au dépôt et à la diffusion de documents scientifiques de niveau recherche, publiés ou non, émanant des établissements d'enseignement et de recherche français ou étrangers, des laboratoires publics ou privés.

1 **Projected future changes in tropical cyclone-related wave climate in the North Atlantic**

2
3 Ali Belmadani¹ (ORCID 0000-0002-4081-8638), Alice Dalphin², Fabrice Chauvin³ (ORCID
4 0000-0001-6071-7212), Romain Pilon^{1,*} (ORCID 0000-0002-3898-1372), Philippe Palany¹

5
6
7
8
9
10
11 (1) Direction Interrégionale Antilles-Guyane, Météo-France, Fort-de-France, Martinique, France

12 (2) Direction des Opérations, Prévision Marine, Météo-France, Toulouse, France

13 (3) Centre National de Recherches Météorologiques, Météo-France/CNRS, Toulouse, France

14 * Now at Laboratoire de Météorologie Dynamique, Institut Pierre-Simon Laplace, Sorbonne
15 Université/CNRS/École Normale Supérieure-PSL Research University/École Polytechnique-IPP,
16 Paris, France

17
18
19
20
21
22
23
24
25
26
27
28
29
30
31
32
33
34
35
36
37
38
39
40
41
42
43
44
45
46
47
48
49 Corresponding author: Ali Belmadani (ali.belmadani@meteo.fr), Météo-France, route du Général
50 Brosset, Morne Desaix, BP645, 97262 Fort-de-France cedex, France

51 **Abstract**

52

53 Tropical cyclones are a major hazard for numerous countries surrounding the tropical-to-subtropical
54 North Atlantic sub-basin including the Caribbean Sea and Gulf of Mexico. Their intense winds,
55 which can exceed 300 km.h^{-1} , can cause serious damage, particularly along coastlines where the
56 combined action of waves, currents and low atmospheric pressure leads to storm surge and coastal
57 flooding. This work presents future projections of North Atlantic tropical cyclone-related wave
58 climate. A new configuration of the ARPEGE-Climat global atmospheric model on a stretched grid
59 reaching $\sim 14 \text{ km}$ resolution to the north-east of the eastern Caribbean is able to reproduce the
60 distribution of tropical cyclone winds, including Category 5 hurricanes. Historical (1984-2013, 5
61 members) and future (2051-2080, 5 members) simulations with the IPCC RCP8.5 scenario are used
62 to drive the MFWAM (Météo-France Wave Action Model) spectral wave model over the Atlantic
63 basin during the hurricane season. An intermediate 50-km resolution grid is used to propagate mid-
64 latitude swells into a higher 10-km resolution grid over the tropical cyclone main development
65 region. Wave model performance is evaluated over the historical period with the ERA5 reanalysis
66 and satellite altimetry data. Future projections exhibit a modest but widespread reduction in
67 seasonal mean wave heights in response to weakening subtropical anticyclone, yet marked increases
68 in tropical cyclone-related wind sea and extreme wave heights within a large region extending from
69 the African coasts to the North American continent.

70

71 **1. Introduction**

72

73 Tropical cyclones (hereafter TCs) are a major hazard for numerous countries surrounding the
74 tropical-to-subtropical North Atlantic sub-basin including the Caribbean Sea and Gulf of Mexico.
75 According to the World Meteorological Organization (WMO), they accounted for over half of all
76 hydrometeorological and climate-related disasters reported in North America, Central America and
77 the Caribbean during recent decades, and for as much as 72% and 79% of the associated deaths and
78 economic losses, respectively (WMO 2014). The Saffir-Simpson scale has been used since the
79 1970s to classify Atlantic TCs according to their intensity, estimated at any given time with their
80 maximum 10-m sustained wind speeds, and is related to potential damage on infrastructure. Yet, it
81 is now known that strong winds are responsible for less than 10% of TC-related deaths in the
82 United States, while nearly 90% are due to water-related incidents: storm surge (49%), heavy rain
83 (27%), hazardous sea and surf in nearshore waters (6%) and further offshore (6%) (Rappaport
84 2014). Thus about 6 fatalities out of 10 are induced by the marine response to TCs, where storm
85 waves play a key role both directly and indirectly through their contribution to storm surge called
86 wave set-up (*e.g.* Harris 1963, Komar 1998).

87 Further, wave run-up, which is the maximum height of instantaneous coastal water levels, is due to
88 water intrusions over the swash zone and onto the beach slope induced by wave breaking and set-up
89 (Stockdon et al. 2006, 2014). Particularly large run-ups caused by major hurricanes with wind
90 speeds of up to 300 km.h^{-1} or more can provoke coastal inundation and induce severe damage to
91 coastal infrastructure and ecosystems (Rey et al. 2019). In a context of climate change associated
92 with inevitable global-scale sea level rise (Church et al. 2013) and a possible increase in the
93 frequency of major hurricanes (Christensen et al. 2013), adaptation measures along coastlines of the
94 world ocean, and the North Atlantic in particular, therefore require an assessment of future
95 projections of TC-related wave climate.

96 The number of studies dedicated to global and basin-scale wave climate projections has markedly
97 increased over the last decade (Mori et al. 2010, 2013, Fan et al. 2013, 2014, Hemer et al. 2013a,
98 Semedo et al. 2013, 2018, Wang et al. 2014, 2015, Guo et al. 2015, Shimura et al. 2015, Hemer and
99 Trenham 2016, Camus et al. 2017, Kishimoto et al. 2017, Timmermans et al. 2017, Vousdoukas et
100 al. 2018a,b, Webb et al. 2018, Morim et al. 2018), particularly in the framework of the Coordinated

101 Ocean Wave Climate Project (COWCLIP, Hemer et al. 2014, 2018) WMO and Intergovernmental
102 Oceanographic Commission (IOC) joint working group (Hemer et al. 2013b, Morim et al. 2019).
103 The latter studies have compiled numerous individual studies to report robust future trends at the
104 global scale across large community-based multimodel ensembles, and to quantify the associated
105 uncertainties due to global climate model (GCM) wind forcing, wave modeling, and emission
106 scenarios (Morim et al. 2019). While there is no doubt that such multimodel approaches provide
107 invaluable information to decision makers as they significantly improve our confidence in wave
108 climate projections, they also suffer from relatively coarse resolutions for modelled wave fields
109 ($\sim 1^\circ$) and GCM wind forcings ($1\text{-}2^\circ$). This is a strong limitation for the assessment of TC-induced
110 wave extremes (Wehner et al. 2015, Timmermans et al. 2017).

111 Indeed, while some GCMs exhibit weak TC-like vortices (Scoccimarro et al. 2011), resolutions of
112 35-50 km are necessary to improve their representation, although with limited performance for
113 major hurricanes (Chauvin et al. 2006, Jullien et al. 2014). Recent research suggests that resolutions
114 of 25 km and higher are needed to fully resolve the observed distribution of TC intensity (Wehner et
115 al. 2015, Chauvin et al. 2020) and associated wave extremes (Timmermans et al. 2017). Therefore,
116 while most of the aforementioned global- and basin-scale studies report on projected changes in
117 extreme wave heights (*e.g.* Fan et al. 2013, Semedo et al. 2013, Guo et al. 2015), their conclusions
118 remain questionable in TC regions.

119 A few exceptions include the 20-km and 25-km winds used by Mori et al. (2010) and Timmermans
120 et al. (2017), respectively. The former study however used a rather coarse 1.25° wave model, which
121 is also likely to bias TC wave extremes compared to the 25-km model implemented by
122 Timmermans et al. (2017), as demonstrated by Chen et al. (2018). The study by Timmermans et al.
123 (2017), which represents the state of the art for global projections of TC-related wave climate,
124 suggests possible large increases in extreme wave height in areas such as the tropical central and
125 eastern North Pacific. Nevertheless, the patterns of expected future changes were noisy and clearly
126 influenced by individual TCs, particularly in the Atlantic, because of the relatively short 23-year
127 simulations, leaving the response of Atlantic TC wave climate to global warming as an open
128 question. Alternative approaches include parametric TC winds (Krien et al. 2018, and references
129 therein) that provide reasonably realistic and computationally cost-effective high-resolution forcing,
130 combined with synthetic TCs statistically downscaled from GCMs under various climate scenarios
131 (*e.g.* Emanuel et al. 2013). However, the high-resolution wave models and associated computational
132 burden remain limiting factors, restricting this approach to regional studies (Appendini et al. 2017).
133 Here we use ARPEGE-Climat, an atmospheric GCM with a stretched grid reaching 14 km
134 resolution in the tropical North Atlantic (Chauvin et al. 2020). It forces a 10-km regional wave
135 model, embedded into a 50-km wave model of the Atlantic Ocean, to infer projected future changes
136 in North Atlantic TC-related wave climate. Unlike Timmermans et al. (2017), 30-year ensemble
137 simulations generate a sufficient number of TCs to infer some robust changes in hurricane wave
138 climate and extreme wave heights. In addition, dynamical downscaling is used to assess the
139 sensitivity of our projections to resolution of winds and waves in the TC main development region
140 (hereafter MDR).

141 The atmospheric GCM simulations are forced with sea surface temperature (SST) from a single
142 IPCC (Intergovernmental Panel on Climate Change) CMIP5 (Coupled Model Intercomparison
143 Project phase 5) coupled GCM under a single RCP8.5 greenhouse gas (GHG) emission scenario.
144 Most projected changes in TC activity found in this model however tend to be consistent with
145 previous studies (Chauvin et al. 2020). In particular: increased proportion and intensity of Category
146 4 and 5 hurricanes, reduced total TC numbers, and a slight shift of TC activity towards the mid-
147 latitudes. Fig. 1 illustrates the latter two as a reduction in the frequency of TC days over most of the
148 North Atlantic including the Caribbean Sea and Gulf of Mexico, and an increase in the $40\text{-}50^\circ\text{N}$
149 band, although now regarded as barely significant after accounting for the multiple-testing problem
150 (Online Resource 1, section 1). It also exhibits a strong, robust increase in TC numbers around Cape

151 Verde extending into the MDR, particularly at the hurricane season peak in September (not shown).
152 This had not been reported before and has been attributed to expected changes in African easterly
153 wave activity (Chauvin et al. 2020). Our results show that TC-related wave climate is sensitive to
154 these projected changes in TC activity, both in the MDR and the extratropics.
155 The present paper is organized as follows. The model and observed datasets and the methodology
156 are detailed in section 2. The results for model evaluation against historical data and for projected
157 future changes in seasonal mean, TC-mean and extreme wave climate are presented in section 3.
158 Section 4 is a discussion of the limitations of our study. Finally, concluding remarks are drawn in
159 section 5.

160

161 **2. Data and methods**

162

163 **2.1. Model and observed data**

164

165 **2.1.1. ARPEGE-Climat atmospheric general circulation model**

166

167 Wind fields from a high-resolution atmospheric GCM are used to drive a wave model of the
168 Atlantic basin and a nested high-resolution model of the MDR. The GCM is ARPEGE-Climat
169 (Batté and Déqué 2016), the atmospheric component of the CNRM-CM CMIP coupled GCM
170 developed at Météo-France, the French national weather service. ARPEGE-Climat offers the
171 capability of a stretched grid, increasing the resolution over a given region at the computational cost
172 of a standard coarse-resolution GCM, thanks to degraded resolution over the antipodes. In addition
173 to numerous climate studies, it has been combined with ocean wave models to perform wave
174 climate projections around France on a 60-80 km stretched grid (Charles et al. 2012) and on a
175 uniform 50 km grid (Laugel et al. 2014). Its CMIP5 coupled coarse-resolution configuration (1.4°),
176 CNRM-CM5, was among the GCMs used in the multimodel wave climate projection studies by
177 Wang et al. (2014), Hemer and Trenham (2016), Camus et al. (2017), and Morim et al. (2019).

178 Here we use a new configuration of ARPEGE-Climat that is being used for CMIP6 within the
179 CNRM-CM6 coupled GCM (Voldoire et al. 2019, Roehrig et al. 2020), except for a stretched grid
180 reaching ~14 km resolution to the north-east of the Lesser Antilles (Cantet et al. 2020). The model,
181 its configuration and the associated climate simulations have been described in detail by Chauvin et
182 al. (2020), so only a brief description is provided here.

183 ARPEGE-Climat has been forced with monthly SSTs from CNRM-CM5 under historical and
184 RCP8.5 climates. SSTs from the historical simulations over 1965-2013 (hereafter Hist-Model) were
185 previously corrected with HadISST1 observed monthly SSTs (Rayner et al. 2003) to ensure
186 unbiased mean climatology, while the same correction was applied to SSTs from RCP8.5
187 simulations over 2031-2080 for consistency. ARPEGE-Climat has also been forced with HadISST1
188 SSTs over 1965-2014 (hereafter Hist-Obs) for the purpose of model comparison with observations.
189 For each of these three climate experiments, 5 ensemble members differing only by their initial
190 conditions allow reaching robust statistics regarding TC-related extremes (Chauvin et al. 2020).
191 Thanks to high resolution, the model is able to represent the distribution of TC winds fairly well,
192 including Category 5 hurricanes (Chauvin et al. 2020).

193 Six-hourly 10-meter winds from the climate experiments (Hist-Obs, Hist-Model, and RCP8.5) with
194 five members each (15 simulations in total) were interpolated onto regular 10-km and 50-km grids
195 over the MDR and whole Atlantic Ocean, respectively, to drive ocean wave models (2.1.2). Such
196 forcing, as well as wind field analysis were considered over the reduced 1984-2013 (Hist-Obs, Hist-
197 Model) and 2051-2080 (RCP8.5) periods (see details in 2.1.2). Winds at different vertical levels and
198 other atmospheric variables were also interpolated onto a 15-km grid over most of the North
199 Atlantic for the full fifty-to-sixty-year time slices in order to apply an automated TC tracking
200 algorithm (Chauvin et al. 2020). The results have been used by Chauvin et al. (2020) to provide TC

201 counts and climatology, as well as related projected future changes. We use some of that
202 information (over the reduced 30-year periods) to define the hurricane season (2.2.1) and extract
203 TC-related wave climate (2.2.2) and extreme wave heights (2.2.3). The ARPEGE-Climat
204 experimental setup and grid characteristics are summarized in Tables 1 and 2, respectively.

205 206 **2.1.2. MFWAM spectral wave model**

207
208 We make use of the MFWAM (Météo-France Wave Action Model) spectral wave model, a version
209 of the WAM (WAMDI Group 1988) developed at Météo-France. MFWAM is a third generation
210 wave model that computes the evolution of sea state in the spectral space thanks to the energy
211 balance equation. It uses the ECWAM-IFS-38R2 code with a dissipation term developed by
212 Ardhuin et al. (2010) and upgraded for the Copernicus Marine Environment Monitoring Service
213 (CMEMS). This term involves the computation of the wave-supported stress from the model
214 spectrum, which is used to modify wind friction velocity and ultimately wind stress through the
215 wave-supported stress effect on sea surface roughness. Such parameterization reduces the drag
216 coefficient and wind input for high wind speeds (Ardhuin et al. 2010), which is relevant for TCs
217 because wave growth would otherwise be overestimated (Powell et al. 2003). The wave spectrum is
218 discretized in 24 directions and 30 frequencies, from 0.035 Hz to 0.58 Hz (1300 m to 5 m
219 wavelengths).

220 The model applies watershed partitioning to split the wave spectrum into wind sea and various
221 swell components. In the first step, the part of the wave spectrum where wind speed exceeds phase
222 speed and wave propagation is aligned with surface winds is considered wind sea. A cosine factor is
223 used to treat neighboring wave directions. The swell part is then partitioned to retrieve sea states of
224 various origins. According to Hasselmann et al. (1996), wave spectra may be considered inverted
225 catchment areas, allowing the use of hydrological methods like the watershed algorithm. Each
226 secondary maximum in the direction-frequency spectrum is thus considered a separate sea state.
227 The most energetic is named primary swell, the second is secondary swell, and so on.

228 Several MFWAM configurations run every day at Météo-France. They are used to issue high surf
229 advisories, watches and warnings for the open ocean and coastal areas. The MFWAM global
230 configuration is also dedicated to CMEMS wave products (Aouf 2018).

231 Our configuration is derived from an operational setup with a 10-km regional grid for the Lesser
232 Antilles and French Guiana (hereafter MFWAM01) nested in a 50-km global grid (MFWAM05). To
233 reduce the computational burden associated with long ensemble simulations, and recognizing that
234 distant swells from other basins have little influence on North Atlantic sea states (Alves 2006,
235 Semedo et al. 2011), the MFWAM05 domain was restricted to the Atlantic (59.5°S-70°N, 99°W-
236 21°E). The South Atlantic was included to allow the propagation of Southern Hemisphere swells
237 into the North Atlantic, particularly in its eastern part as inferred from comparison to an experiment
238 with the model southern boundary located at 10°S (not shown). We however excluded the latitudes
239 north of 70°N where local swells are unlikely to influence lower latitudes in any significant way.
240 For simplicity, sea ice was not taken into account. Although not global, the MFWAM05
241 configuration was only forced at the surface with ARPEGE-Climat winds without any prescribed
242 wave spectra along the open boundaries.

243 The MFWAM01 domain was extended eastwards to make the most of highest-resolution MDR
244 winds (5°N-28°N, 75°W-10°W). Three-hourly MFWAM05 spectra were prescribed at the open
245 boundaries for remote swell propagation into the MFWAM01 domain. MFWAM01 wave spectra
246 were however not fed back into the MFWAM05 domain (one-way nesting). Our purpose is to assess
247 the sensitivity of our results to the resolution of winds and waves (in the MDR), rather than
248 upscaling effects from the MDR to basin scale, which would require 2-way nesting. Table 2
249 summarizes the MFWAM nested grid configuration.

250 Since our focus is on TC-related wave climate, and given the high computational costs of dynamic
 251 wave model simulations for the whole calendar year over fifty-to-sixty-year periods with available
 252 ensemble wind data, temporal and seasonal subsampling had instead to be applied. For each climate
 253 experiment and ensemble member (Table 1), only the last 30 years were considered. This is a trade-
 254 off between numerical cost and periods long enough to minimize natural low-frequency variations,
 255 thus isolating the anthropogenic global warming signal. For RCP8.5 wave simulations (hereafter W-
 256 RCP8.5), we focus on long-term projections after the mid-21st century (2051-2080) and thus on the
 257 potentially largest changes. For W-Hist-Model and W-Hist-Obs simulations forced with Hist-Model
 258 and Hist-Obs winds (1984-2013), the pre-satellite era (before 1979) is excluded, guaranteeing
 259 observations of the highest possible quality for model calibration and validation (see 3.1). In
 260 addition, only the hurricane season (about 4 months from July to November, see 2.2.1) was
 261 simulated each year for the 15 available ARPEGE-Climat simulations (Table 1). Therefore, 450
 262 simulations were run for MFWAM05 and MFWAM01. The analysis considers three-hourly outputs
 263 for significant wave height H_s , mean wave period T_m , and H_s partitioning into wind sea and primary
 264 swell (H_{s0} and H_{s1} , respectively). Table 3 summarizes the MFWAM experimental setup.

265 2.1.3. Reanalysis and altimetry wind and wave data

266
 267
 268 The European Centre for Medium-Range Weather Forecasts (ECMWF) ERA5 reanalysis (Hersbach
 269 et al. 2020) is used as a reference to assess surface winds in the ARPEGE-Climat Hist-Obs runs
 270 over the North Atlantic. Specifically, 6-hourly 10-meter winds (interpolated at 0.5° resolution) over
 271 the 1984-2013 hurricane seasons (July 9 to November 9, see 2.2.1) and their standard deviation are
 272 compared to those from the 5-member GCM archive (Table 1).

273 ERA5 features an ocean wave component coupled with the atmospheric reanalysis called ECWAM
 274 (European Centre Wave Action Model), which is the ECMWF version of WAM with a dynamical
 275 core similar to MFWAM. Similarly to surface winds, 6-hourly outputs are interpolated at 0.5°
 276 resolution. They are used to assess the MFWAM05 and MFWAM01 model performance in terms of
 277 mean H_s and T_m as well as their standard deviation. On the other hand, the older ERA-Interim
 278 reanalysis (Dee et al. 2011) was used to calibrate MFWAM in terms of the wave growth coefficient
 279 β_{max} to minimize model bias (see 3.1.2). ERA5 could not be used because the data was not yet
 280 available over the entire 1984-2013 period when the MFWAM simulations were performed.
 281 However, our calibration appears reasonable in the light of the comparison of model bias relative to
 282 ERA5 and altimetry data (3.1.2).

283 To assess the uncertainty in observed wave climate, MFWAM mean H_s and its standard deviation
 284 were also compared to those from the remotely-sensed ESA CCI (European Space Agency Climate
 285 Change Initiative) Sea State 1° monthly level-4 multimission product version 1.1 (Piolle et al. 2020,
 286 Dodet et al. 2020). The comparison was performed over the available 1991-2013 record and the
 287 months of August to October (ASO). This is the longest sequence of complete months within the W-
 288 Hist-Obs hurricane season. The base data are the median H_s values over each satellite track portion,
 289 within each 1° bin over a one-month period. They are hereafter referred as h_{mp} ($p=1, \dots, n_m$), where
 290 n_m is the number of such values for each month m . Various statistics particularly suitable for wave
 291 climate studies are provided (Timmermans et al. 2020, Dodet et al. 2020). ASO mean significant
 292 wave height \bar{H}_s was estimated by ensemble-averaging the 69 available monthly averages of h_{mp} . For
 293 each month m , the sum of squared h_{mp} and n_m are also available. The ASO standard deviation of H_s
 294 over 1991-2013 was then estimated as :

$$295 \quad \sigma = \sqrt{\frac{1}{N} \sum_{m=1}^{69} \sum_{p=1}^{n_m} h_{mp}^2 - \bar{H}_s^2}, \quad (1)$$

297 where $N = \sum_{m=1}^{69} n_m$ is the total number of median H_s values over the entire period.

298

299

2.2. Methods

300

301 In this section, the methodologies used to estimate the hurricane season dates and to extract mean
302 and extreme TC wave climate are presented. The statistical methods used to assess sampling
303 uncertainties in our projections are detailed in the Online Resource 1.

304

305

2.2.1 Estimation of the hurricane season

306

307 According to WMO, the Atlantic hurricane season officially extends from June 1 to November 30.
308 Yet, it was not necessarily appropriate to consider these dates. Indeed, our projections of TC-related
309 wave climate are driven by climate models that are not able to reproduce the exact dates of the
310 hurricane season. In addition, shifts in the season dates are expected (see 3.2). Since statistics over
311 the W-Hist-Model and W-RCP8.5 hurricane seasons are compared, it requires independent
312 definitions for historical and future seasons. Last, for matters of computational cost, a less
313 conservative definition was sought to reduce season length. The use of fixed, standard dates may
314 however be useful for matters of reproducibility (section 4.6).

315 For each climate experiment (Hist-Obs, Hist-Model, RCP8.5), the hurricane season was defined as
316 the period of the year when at least 30 so-called TC days were found for each calendar day among
317 the 150-year multimember archive (Table 3). A given date is a TC day if at least one TC was
318 detected in the North Atlantic sub-basin with the methodology of Chauvin et al. (2020). Therefore,
319 the hurricane season is the time of the year with TC daily return period below 5 years.

320 Projected changes in extreme TC-related wave heights over the season peak when TC activity is
321 highest are also of interest. Unlike the previous approach based on TC track data, we focus here on
322 return periods of extreme wave heights directly as diagnosed from MFWAM01. To provide
323 meaningful results in terms of potential impacts on coastal human settlements and ecosystems, the
324 analysis is restricted to a region around the Lesser Antilles in the eastern Caribbean. Indeed, these
325 small islands are the first landmasses crossing the path of TCs generated in the MDR.

326 Let $p(H_{S_{\max}} \geq 3 \text{ m})$ be the occurrence probability that the MFWAM01 maximum H_s over the eastern
327 Caribbean (11.7-19°N, 59-64°W) exceeds 3 m for any given calendar 3-hourly time step among the
328 30-year, 5-member archive. The hurricane season peak was then arbitrarily defined as the period
329 when $p(H_{S_{\max}} \geq 3 \text{ m}) \geq 4.5\%$ (on average every 1.35 years out of 30). It is thus the time of the year
330 with 3-hourly return period of these extreme events below ~ 22 years. Thresholds of 2 m and 4 m
331 captured events that were respectively too frequent - thus neither extreme nor necessarily TC-
332 related - and too rare, leading to noisy and not robust results (not shown).

333

334

2.2.2. Estimation of TC-related wave climate

335

336 One question addressed here is how the contribution to mean ocean wave climate of all TCs taken
337 together (from tropical storms to major hurricanes), hereafter referred to as TC-related wave
338 climate, is likely to change under a RCP8.5 scenario. Therefore, one needs to estimate TC-related
339 wave climate in W-Hist-Model and W-RCP8.5. For a given parameter (H_s , H_{s0} , H_{s1} , T_m), the first
340 step is to compute a composite average over all the TC days identified in the 150 model runs for
341 each experiment (Table 3). More accurately, the average is computed over all the 3-hourly outputs
342 included within TC days: 58845 and 52861 time steps in total for the 5 members of W-Hist-Model
343 and W-RCP8.5, respectively. This is performed at every grid point with all time steps weighted
344 equally.

345 However, this is not representative of mean TC-related wave climate because on any given TC day,
346 TC conditions will only dominate over a fraction of the sub-basin. Sea states in other regions may
347 be influenced by various drivers such as remote swells of extratropical origin, trade wind swells,
348 local wind sea etc. In fact, composite averages appear similar to seasonal means because TCs are
349 sufficiently rare at any given location for their average contribution to be minor. To reveal it, one
350 thus needs to remove the hurricane-season mean field (*i.e.* averaged over both TC and non-TC days
351 from the 150 simulated seasons) from the composite field (averaged over TC days only). It is
352 assumed that other wave drivers are mostly uncorrelated with TCs and therefore not much different
353 on average on TC and non-TC days. The derived anomalous field then represents TC-related wave
354 climate, and the difference between the corresponding W-RCP8.5 and W-Hist-Model fields
355 represents its future evolution.

356 **2.2.3. Estimation of extreme TC-related wave heights**

359 In addition to the contribution of all TCs to ocean wave climate, the wave response to expected
360 changes in extreme TCs is also of interest. While many extreme wave height events during the
361 hurricane season are induced by TCs, mid-latitude swells may also drive large waves, especially
362 towards the season end (October and November) that coincides with autumn and seasonal increases
363 in the frequency and strength of mid-latitude low-pressure systems. To filter out such non TC-
364 related wave extremes, only TC days are considered.

365 Following Wang et al. (2014), extreme TC-related H_s are estimated according to extreme value
366 analysis. Independent and identically distributed realizations, which are necessary to compute
367 unbiased statistics (Online Resource 1, section 4), are obtained by only retaining the annual
368 maximum value of H_s over TC days for each model grid point. In the rare cases with no TC days for
369 a given year and ensemble member, which only occurred when the computation was restricted to
370 the hurricane season peak (section 3.2.3), the annual maximum H_s is taken over non-TC days (4 and
371 2 instances out of 150 for W-Hist-Model and W-RCP8.5, respectively). A Generalized Extreme
372 Value (GEV) distribution is then fit to the resulting 150-value sample (Table 3) at each grid point,
373 from which a 10-year return level and its associated 95% confidence interval are derived. As
374 detailed in the Online Resource 1 (section 4), the statistical significance of the associated projected
375 changes is assessed considering any overlap between the confidence intervals from W-Hist-Model
376 and W-RCP8.5.

377 **3. Results**

378 **3.1. Atmospheric and wave model performance**

380 **3.1.1. ARPEGE-Climat model performance**

383 ARPEGE-Climat TC track analysis (see 2.2.1) yields the following model hurricane season dates:
384 July 9 to November 9, July 6 to November 10, and July 20 to November 3 for Hist-Obs, Hist-
385 Model, and RCP8.5, respectively (Fig. 2). Repeating with IBTrACS best-track data (Knapp et al.
386 2010) over 1984-2013 yields a season extending from July 5 to November 13. Hist-Obs and Hist-
387 Model thus represent the hurricane season timing fairly well. ARPEGE-Climat however
388 underestimates the number of TC days during the hurricane season, particularly around the season
389 peak early September, while overestimating it off season (see also Chauvin et al. 2020, Cantet et al.
390 2020).

392 We then assess patterns of mean present-climate hurricane-season wind forcing using ERA5 as a
393 reference. Hist-Obs features realistic low-level circulation compared to reanalysis data (Fig. 3ab).
394 The subtropical anticyclone is however weaker with a systematic bias of $\sim -1 \text{ m.s}^{-1}$ (Fig. S2), which

395 possibly results from the lack of data assimilation in the GCM. In contrast, surface wind standard
396 deviation is overestimated by 20-30% across the sub-basin, particularly between the US East Coast
397 and the Azores Islands (Fig. 3c). On the other hand, a slight underestimation (5-10%) is visible near
398 5-10°N between Africa and the Lesser Antilles. In fact, the standard deviation bias pattern appears
399 quite similar to present-climate frequency of TC days (black contours on Fig. 1), suggesting it may
400 result from large TC activity in the subtropics compared to ERA5. Indeed, this is consistent with
401 more TCs in the extratropics and less in the MDR compared to best-track data (Chauvin et al.
402 2020). Such data is however subject to some uncertainty (Knapp et al. 2010) and the relatively low-
403 resolution reanalysis (native resolution is ~30 km) cannot adequately grasp TC wind speeds, which
404 may explain part of the model bias in the standard deviation. The secondary maximum at 15-20°N
405 in standard deviation bias (Fig. 3c) may result from very strong TC winds compensating
406 underestimated MDR TC numbers (Chauvin et al. 2020). Noteworthy, the comparison of ERA5 and
407 Hist-Model (instead of Hist-Obs) yields almost identical bias in mean winds and their standard
408 deviation (not shown).

409 410 **3.1.2. MFWAM model performance**

411
412 More frequent TCs and associated strong winds in the GCM subtropics than in reality trigger overly
413 large waves and long-period swells in MFWAM05. Indeed, extratropical H_s and T_m were initially
414 overestimated in a single-member set of W-Hist-Obs simulations by as much as +0.5-1 m and +1-
415 1.5 s relative to ERA5, respectively (not shown). To compensate for the excessive wind variability,
416 the wave growth coefficient β_{max} was reduced for both MFWAM05 and MFWAM01 after succinct
417 calibration/validation against ERA-Interim from 1.52 (operational configuration) to the value of
418 1.13 also used by Stopa (2018). Positive H_s and T_m biases were thereby reduced almost everywhere
419 and particularly in the extratropics. It appeared difficult to reduce such biases (~+0.4 m and ~+0.5 s,
420 Fig. 4ab) any further because of negative H_s bias of similar intensity in the tropics (Fig. 4a).

421 The comparison of model H_s with altimetry allows us to qualify these results to some extent.
422 Despite the gridded ESA Sea State CCI data being only available over the reduced 23-year record
423 and shorter ASO period shared with the wave model, the associated H_s bias pattern is similar (Fig.
424 S3a). Compared with ERA5, the ESA Sea State CCI mean H_s is larger, consistently with
425 Timmermans et al. (2020) and Dodet et al. (2020). As a result, the MFWAM05 positive (negative)
426 bias in the subtropics (tropics) is reduced (slightly enhanced) when referred to ESA Sea State CCI.
427 Although ESA Sea State CCI level-4 data is gridded at 1°, it is mostly a collection of 1-Hz
428 alongtrack measurements with careful quality control and extensive calibration against wave buoys.
429 As such, it is considered at least as reliable as ERA5 H_s data, which underestimate buoy
430 observations at various locations including the northwestern Atlantic (Timmermans et al. 2020).
431 Overall ERA-Interim appears as a reasonable choice for MFWAM05 calibration, other datasets
432 revealing that biases are modest in H_s , although significant in T_m .

433 After calibration, the pattern of MFWAM05 H_s standard deviation is reasonable, featuring a marked
434 increase with latitude similarly to mean H_s (not shown). However, H_s standard deviation is also
435 overestimated in the extratropics by as much as 50-60% compared to ERA5. This most likely
436 results from the overestimated wind variability, judging from the striking similarity in the respective
437 bias patterns. See for example the positive and negative biases near 30-40°N/40-50°W and 5-
438 10°N/15-50°W, respectively (Fig. 3c, 4c). Satellite estimates confirm the excessive extratropical H_s
439 variability though with weaker bias, while weak negative biases are found over the tropics and high
440 latitudes (Fig. S3b). More variable mid-latitude wave heights than in the real ocean induce more
441 variable swell periods in the tropics and along the sub-basin boundaries by up to 50% (Fig. 4d).
442 Noteworthy, the overestimated T_m variability tends to concentrate in the MDR and along the US
443 East Coast, right around the model TC region (Fig. 1). Overall, these findings suggest that our

444 calibration, which is driven by a reduction in mean biases, does not necessarily lead to systematic
445 overestimation of sea state variability (and possibly of extreme wave heights).

446

447

3.2. Projected future changes

448

449

3.2.1. Seasonal mean wave climate

450

451 First of all, one may note a slight shortening of the hurricane season that starts two weeks later and
452 ends one week earlier in the future projections (Fig. 2). In ARPEGE-Climat under RCP8.5, trade
453 winds and westerlies slow down by $0.5\text{-}1.5\text{ m}\cdot\text{s}^{-1}$, as shown on Fig. 5a by blue shading together with
454 westerly and easterly wind vector anomalies near 10°N and 50°N , respectively. These differences in
455 U10 between the two ensembles are significant at the 5% level, as indicated by hatchings over most
456 of the sub-basin. Such weakening of the subtropical anticyclone is accompanied by slight poleward
457 migration of low-level circulation: zonal bands of positive wind speed anomalies in the subtropics
458 and high latitudes are found to the north of the weakening easterly trade winds and westerlies,
459 respectively. This is consistent with previously reported poleward widening and weakening Hadley
460 cell with global warming (Johanson and Fu 2009, Gastineau et al. 2009), and specifically,
461 decreasing wind speeds in the North Atlantic mid-latitudes (Kar-Man Chang 2018).

462 Weaker future winds trigger moderate yet robust 5-10% sub-basin-wide reduction in H_s ,
463 particularly in the mid-to-high latitudes and east of the Lesser Antilles (Fig. 5b), in general
464 agreement with CMIP3 and CMIP5 multimodel studies (Hemer et al. 2013b, Morim et al. 2019).
465 Conversely, projected changes in T_m are weak over most of the sub-basin, except for a significant
466 reduction along numerous coastal regions across the North Atlantic (Fig. 5c), possibly in response
467 to weaker distant swells in W-RCP8.5.

468 The reduction in H_s extends over the entire hurricane season (Fig. 6a-c). It is however smallest and
469 not statistically significant in late August and September, both in the mid-latitudes (Fig. 6a) and
470 tropics (Fig. 6bc). The reduction in mean H_s may be partly compensated by maximum increases in
471 TC-related extreme wave heights at the hurricane season peak (see section 3.2.3). Downward trends
472 in mean H_s are evident in the mid-latitudes, $\sim\text{-}1\text{ cm/decade}$ and $\sim\text{-}2.5\text{ cm/decade}$ for W-Hist-Model
473 and W-RCP8.5, respectively, and in the eastern Caribbean with $\sim\text{-}1\text{ cm/decade}$ for W-RCP8.5 (Fig.
474 7). They are however modest compared with year-to-year variations and inter-member spread:
475 standard deviation and confidence interval width range from 3 to 10 cm and from 6 to 12 cm,
476 respectively. These results exhibit little sensitivity to horizontal resolution of wind and waves, at
477 least in the MDR and eastern Caribbean that are included in the MFWAM01 domain (Fig. 8ab).
478 This is because projected changes in seasonal means mostly result from changes in large-scale
479 atmospheric patterns as argued here.

480

481

3.2.2. TC-related wave climate

482

483 The spatial pattern of W-Hist-Model TC-related H_s (*i.e.* the hurricane-season mean contribution of
484 TCs to H_s , contours on Fig. 9a) is qualitatively similar to the Hist-Model frequency of TC days
485 (contours on Fig. 1), suggesting that the methodology described in 2.2.2 is adequate. Indeed, TC-
486 related wave heights are highest around Bermuda near $30\text{-}35^\circ\text{N}$, 65°W ($\sim\text{0.45 m}$ *i.e.* $\sim\text{25\%}$ of mean
487 H_s) and extend from the tropics to the mid-latitudes, particularly in the sub-basin western half.
488 Compared to TC activity (Fig. 1), the H_s pattern is somewhat smoother and more isotropic (Fig. 9a).
489 This is mostly because of swell propagation away from TC-induced wind fetches. The
490 corresponding H_{s0} pattern is more zonal and closer to TC-day frequency (Fig. 9b, contours)
491 compared to the wider and smoother H_{s1} pattern (Fig. S4a, contours): meridional scales are $\sim\text{3500}$
492 km and $\sim\text{2000 km}$ for H_{s1} and H_{s0} , respectively, as inferred from the 0.05 m contour.

493 The pattern of projected future changes in TC-related H_s (shading on Fig. 9a) is also somewhat
494 similar to changes in TC activity (shading on Fig. 1), with widespread 2-5 cm reduction across the
495 sub-basin and 3-4 cm increases off the African continent and northeastern United States. However,
496 notable differences are found. The increase off Cape Verde extends all the way across the MDR into
497 the Caribbean Sea, while that off New England does not extend across the sub-basin mid-latitudes,
498 unlike the increase in TC activity (Fig. 1). Even more importantly, the projected changes in TC-
499 related H_s are not statistically significant. This is also the case for H_{s1} (Fig. S4a) and T_m (Fig.
500 S4b), but not for H_{s0} , which exhibits a significant 2-5 cm increase across most of the MDR (Fig.
501 9b). Although a closer relationship with wind changes is expected for H_{s0} compared to other
502 variables, this finding is somewhat surprising, as these changes extend much farther west compared
503 to those in TC frequency (Fig. 1). Projected changes in TC activity only considered the locations of
504 TC centers (Chauvin et al. 2020) and not the large associated wind fetches considered in H_{s0} , which
505 may be one explanation. Alternatively, TCs around Cape Verde may be associated with background
506 conditions that favor enhanced U_{10} in the trade wind belt.
507 Conversely to mean wave heights, expected changes in TC-related wave heights show some
508 sensitivity to spatial resolution of winds and waves. Indeed, while the magnitude of projected
509 changes in MDR TC-related H_{s0} is similar in MFWAM01 (Fig. 9d) and MFWAM05 (Fig. 9b), the
510 former are significant over wider regions. In particular, the increase in MFWAM01 TC-related H_{s0}
511 is significant not only west of Cape Verde but also east of the archipelago all the way up to the
512 African continent. This may be related to small-scale wind changes in the region of sharp increase
513 in TC activity (Fig. 1) being better accounted for in the higher-resolution wave model. On the other
514 hand, projected changes in TC-related H_s , H_{s1} , and T_m are not very sensitive to resolution (Fig. 9ac,
515 S4).

516 517 **3.2.3. Extreme TC-related wave heights**

518
519 In W-Hist-Model, 10-year TC-related H_s during the hurricane season range from 2-3 m in the
520 equatorial Atlantic to 15-16 m near 60°W, 40°N off northeastern United States (contours on Fig.
521 10a). Such a pattern is broadly consistent with mean TC-related H_s (Fig. 9a) but slightly displaced
522 northeastward. Unlike mean TC-related H_s , it also presents a broad, homogeneous pattern of
523 elevated values (10-11 m) north of 50°N. This is likely a residual signal mostly from non-TC-
524 related H_s : 10-year H_s computed over both TC and non-TC days exhibits a secondary maximum
525 near 60°N (not shown). “Post-TCs” resulting from extratropical transitions may also play a role,
526 particularly because of lagged wave response to winds due to wave growth in developing seas and
527 swell propagation after TC decay (see 4.5).

528 Nevertheless, restricting the computation of 10-year TC-related H_s to the season peak yields a
529 sharper decay north of ~45°N while conserving a maximum at 40°N with values ~14 m (contours
530 on Fig. 10b). Indeed, the analysis of MFWAM01 extreme wave heights leads to the definition of the
531 following periods for the season peak (see 2.2.1): August 17 to September 15 for W-Hist-Model and
532 August 17 to September 18 for W-RCP8.5 (Fig. 8d). These findings are consistent with stronger TC
533 activity and weaker mid-latitude storm activity from mid-August to mid-September compared to
534 late hurricane season in October-November. Note that 10-year TC-related H_s are slightly larger
535 when computed over the entire season (Fig. 10ab) because annual maxima occasionally occur
536 outside of the season peak.

537 Repeating the analysis for H_{s1} and H_{s0} yields similar patterns (contours on Fig. S5). The gradient of
538 extreme wave heights between the northwestern part of the basin and the MDR is however larger
539 for H_{s0} compared to H_{s1} : maximum values near 40°N exceed 12/15 m (respectively 8/10 m) for H_{s0}
540 (respectively H_{s1}) over the season peak/whole season, and decrease below 2 m (respectively 3 m)
541 near 5-10°N. Smoother variations in H_{s1} are consistent with hurricane swell propagation over large
542 distances. Interestingly, a secondary maximum near 60°N in 10-year TC-related H_{s0} only arises

543 when the analysis extends over the whole season (Fig. S5c) and is not seen for H_{s1} (Fig. S5ab). It is
544 again consistent with extratropical storm rather than TC forcing north of 45°N .
545 Under RCP8.5 climate, 10-year TC-related H_s , H_{s1} , and H_{s0} increase markedly over the hurricane
546 season near the central and northern US East Coast by up to 2-3 m (shading on Fig. 10a, S5ac),
547 although only limited areas southeast of Cape Hatteras, Cape Cod, and Nova Scotia experience
548 statistically significant changes. Chauvin et al. (2020) found a statistically significant increase in the
549 intensity of major hurricanes over the North Atlantic. However, this result may not apply locally
550 where the largest expected changes in extreme wave heights are found. Indeed, since TC tracks are
551 also projected to change (Chauvin et al. 2020), finding localized robust changes is not
552 straightforward. Instead, projected changes in the spatial structure, lifetime, phase speed or
553 trajectories of major hurricanes might favor more efficient growth as waves propagate away from
554 the storm center, consistently with the wider patch of significant H_{s1} increase (Fig. S5a).
555 A 1-2 m increase in 10-year TC-related H_s is also found within the MDR along a northwest-
556 southeast oriented band extending from Cape Verde to $\sim 60^{\circ}\text{W}$, 20°N , but is only significant near
557 30°W (Fig. 10a). Unlike the increase in the northwestern Atlantic, it is associated with a statistically
558 significant increase in H_{s0} rather than H_{s1} (Fig. S5ac). This is consistent with the strong increase in
559 TC activity around Cape Verde reported by Chauvin et al. (2020) and the significant increase in TC-
560 related H_{s0} in the MDR (Fig. 9bd). Further south and closer to the equator, a robust reduction in
561 extreme H_s , H_{s1} , and H_{s0} is also found. Its extension and orientation are similar to those of the
562 extreme wave height increase, suggesting both may combine to form a dipole, possibly associated
563 with poleward displacement of extreme wave heights. In fact, projected TC frequency changes
564 exhibit a similar dipole (Fig. 1).
565 When the projected changes in extreme wave heights are restricted to the season peak (Fig. 10b,
566 S5bd), they are larger (over 4-m H_s increase off the US East Coast), mostly positive, and more
567 robust in the MDR and northwestern Atlantic. This again is consistent with Chauvin et al. (2020)
568 who found an overall reduction in TC numbers over the season (see the widespread decrease on Fig.
569 1), yet a strong increase in September with a pattern similar to those found for extreme wave
570 heights (Chauvin et al. 2020, their Fig. 10).
571 The comparison of projected changes in MDR 10-year wave heights between MFWAM05 and
572 MFWAM01 illustrates the sensitivity of our results to resolution (see also 3.2.2). The magnitude of
573 these changes is similar in the two grids (Fig. 10) but they are statistically significant over slightly
574 wider areas in MFWAM01. These results are qualitatively consistent with those found for MDR
575 TC-related H_{s0} (Fig. 9bd) and advocate for increased model resolution including wave models, not
576 just the GCMs.
577 Projected changes in the return periods of extreme wave heights depending on the season phase
578 (early season, peak phase, late season) are also of interest. The likelihood that wave heights exceed
579 certain thresholds within the mid-latitudes, MDR, and eastern Caribbean varies through the season
580 (Fig. 6d-f), as anticipated from seasonal variations in TC activity (Fig. 2). For both W-Hist-Model
581 and W-RCP8.5, the frequency of extreme wave heights increases sharply after late July/early
582 August, reaches a maximum a month later, before decaying again in the second half of October. In
583 the eastern Caribbean, extreme wave height frequency rises again in early October (Fig. 6f), which
584 may result from remote swells of extratropical origin rather than TC-related storm waves.
585 Future projections show changes similar to those in TC numbers (maximum number of TC years
586 rises by 7% from ~ 16.2 for Hist-Model to ~ 17.4 for RCP8.5, Fig. 2): a 20-30% increase in August-
587 September in the three regions, although not statistically significant (Fig. 6d-f). The sign of the
588 change in the early and late seasons is however region-dependent: an increase in the mid-latitudes
589 (Fig. 6d), little change in the MDR (Fig. 6e), and a decrease in the eastern Caribbean (Fig. 6f).
590 Although none of these regions exhibits statistically significant increases in extreme wave event
591 frequency during the season peak (Fig. 6d-f), the lack of significance for the concurrent decrease in
592 mean wave heights (Fig. 6a-c) suggests that the increase may be robust. In the tropical North

593 Atlantic, the frequency of wave extremes decreases in October, possibly because of concurrent
594 reductions in the frequency of mid-latitude storms and associated swells. On the other hand, strong
595 interannual variations and inter-member spread in W-Hist-Model and W-RCP8.5 complicate the
596 detection of long-term trends in wave extremes to an even greater extent than mean H_s (Fig. 11):
597 standard deviations are typically ~ 0.02 *i.e.* 45-90% of the mean, and confidence interval width is
598 ~ 0.03 on average.

599 Similarly to mean TC-related H_{s0} and 10-year TC-related H_s (Fig. 9bd, 10), the frequency of
600 extreme wave heights is sensitive to the spatial resolution of winds and waves (Fig. 8cd, S6),
601 particularly within the MDR: extreme H_s values are much more frequent with increased resolution,
602 consistently with Timmermans et al. (2017) and Chen et al. (2018). The associated projected future
603 changes are however still not statistically significant.

604

605 **4. Discussion**

606

607 **4.1. Choice of GCM, prescribed SST, and GHG forcing**

608

609 An obvious limitation to this study is the use of a single combination of GCM, prescribed SST, and
610 GHG emission scenario. Considering more combinations would help better quantify uncertainties,
611 but is beyond the scope of this study because of constraints set by computational cost and lack of
612 resources. Nevertheless, our projections of TC activity are consistent with previous studies. Key
613 results include reduced TC numbers, increased proportion and intensity of major hurricanes,
614 poleward displacement of TC activity to some extent (Chauvin et al. 2020, Fig. 1), and slightly
615 shorter hurricane season (Fig. 2, Table 3, see also Diro et al. 2014). Therefore and despite the
616 uncertainties, our results represent an ocean wave response to projections of TC activity that are
617 consistent with state-of-the-art knowledge.

618

619 **4.2. Wave model calibration and bias correction**

620

621 The use of a single wave model is another important source of uncertainty, which may be reduced
622 with further calibration and improved physics (Morim et al. 2019). In particular, only a partial
623 sensitivity study of H_s bias to the wave growth coefficient β_{max} was conducted and led to the use of a
624 value of 1.13 that is substantially lower than in the operation configuration (1.52, lowered in 2018
625 to 1.48). An intermediate value of 1.30 was tested, but more exhaustive study may have led to
626 slightly larger or lower value than 1.13.

627 Lemos et al. (2020) underlined the importance of bias correction that is widely used in climate
628 impact studies (e.g. Déqué 2007, Cantet et al. 2014) but hardly for wave climate projections
629 (Charles et al. 2012). Using the GOW2 hindcast that reproduces extreme TC wave heights
630 remarkably well (Perez et al. 2017), they show that mean and extreme present-climate H_s can be
631 efficiently corrected, and that future projections are sensitive to such corrections. The authors
632 however considered coarse-resolution GCMs ($1-3^\circ$) and wave models (1°) that cannot grasp the
633 magnitude and small-scale structure of TC winds and waves, unlike our high-resolution models.
634 Therefore, correcting our simulations may not improve TC wave heights as significantly as Lemos
635 et al. (2020) did. Nevertheless, future research should consider calibration and bias correction for
636 further control of model bias and reduced uncertainties.

637

638 **4.3. Lack of ocean/atmosphere/wave coupling**

639

640 Projected changes in extreme H_s are related to those found for major hurricanes by Chauvin et al.
641 (2020). Although ARPEGE-Climat reproduces the distribution of Atlantic TC intensities fairly well,
642 the authors recognize a tendency for overestimation. They argue that it may result from a lack of

643 small-scale air-sea coupling, among other factors such as details of the turbulence scheme (Roberts
644 et al. 2020a). Indeed, uncoupled simulations lack the wind-driven ocean cooling through vertical
645 mixing and upwelling and consequent feedback to the atmosphere (*e.g.* Jullien et al. 2014). The
646 very large changes in extreme H_s expected over parts of the North Atlantic may thus be
647 overestimated. Future work should consider high-resolution coupled GCM forcing, which is starting
648 to become available as high-performance computing continues to progress rapidly (Roberts et al.
649 2020b).

650 Wave-atmosphere coupling is also important for TCs. Chen and Yu (2017) showed that wave
651 simulations driven by Hurricane Katrina (2005) are significantly improved when a wave boundary
652 layer model (WBLM, Moon et al. 2004) is used to compute wind stress, compared to standard bulk
653 formula. MFWAM includes a wind stress parameterization that accounts for wave effects on sea
654 surface roughness and effectively reduces the drag coefficient for high winds (Ardhuin et al. 2010),
655 as expected from TC wind observations (Powell et al. 2003). Its efficiency compared to other
656 parameterizations (*e.g.* WBLM) has however not been assessed and may be improved. For example,
657 introducing a cut-off frequency for the wave spectrum further limits the drag coefficient for strong
658 winds in a newer version of MFWAM (Aouf et al. 2018).

659 Improvements in TC wave projections will continue gradually, incorporating one feedback loop at a
660 time before a fully coupled ocean-atmosphere-wave model may be built.

661

662 **4.4. Child model nesting**

663

664 Our choice for the nested model domain is retrospectively questionable. First, because Chauvin et
665 al. (2020) found that MDR TC numbers are underestimated by a factor two. And second, because
666 the largest increases in extreme H_s were found elsewhere, in the northwestern Atlantic. Future
667 studies shall improve the spatial distribution of TC activity, and downscale wave models right
668 where projected changes in extreme H_s are strongest. Besides, high-resolution runs with either high-
669 or coarse-resolution winds could be used to disentangle the roles of TC wind distributions and
670 small-scale wave processes.

671

672 **4.5. Selection of TC days**

673

674 The chronological approach based on TC days and used to eliminate non-TC related sea states has
675 limitations. For instance, extratropical storms sometimes occur simultaneously with TCs further
676 south, and their effects are erroneously included. Yet, such artefacts are likely modest given the
677 focus on the hurricane season (mid-latitude storms are more active in winter) and the generally
678 uncorrelated tropical and extratropical drivers. An additional complexity is however introduced by
679 the extratropical transition that TCs often undergo during their decaying phase (Bieli et al. 2019a,b).
680 This is particularly true for Chauvin et al. (2020)'s ARPEGE-Climat simulations that overestimate
681 subtropical North Atlantic TC activity.

682 Most previous studies have similar limitations. Fan et al. (2013) and Timmermans et al. (2017)
683 presented projections of extreme wave heights and compared them qualitatively with projected TC
684 activity, without explicit criteria to extract TC wave signals. Appendini et al. (2017) used a
685 methodology similar to ours by computing extremes over each TC event. Their domain was
686 however limited to the Gulf of Mexico, thus focusing on wind sea by construction and avoiding the
687 issue of the attribution to other drivers.

688 An exception is the study of western North Pacific TC wave projections by Shimura et al. (2015),
689 where TC waves are determined from TC center locations considering a 500-km radius. TC tracks
690 were obtained by Murakami et al. (2012) with a methodology similar to ours. Such geolocalization
691 has not been considered here because hurricane swell can propagate over much larger distances
692 (Zelinsky 2019). The benefit of our approach is that extreme wave heights outside TC regions but

693 subject to such remote swells are accounted for. In addition to a residual effect from non-TC-related
694 extremes, the lack of georeferencing may however lead to underestimated TC wave climate and
695 future projection outside TC regions, as suggested by the not statistically significant changes in TC-
696 related H_s and H_{s1} (Fig. 9ac, S4ac).

697 A limitation to both this study and Shimura et al. (2015) is that no delay was considered between
698 TC tracks and associated sea states. Therefore, the propagation of swell generated during TC
699 decaying phase is mostly not accounted for. The solution is not straightforward. Such delay should
700 depend on storm intensity, structure and translation velocity, which affect wind fetches, wave
701 periods and ultimately, swell phase speeds. It was however not considered critical for wave
702 extremes because at most locations over long periods, these should be driven by TC lifetime
703 maximum winds before the decaying phase (except maybe for mid-latitude H_{s0} , Fig. S5c).

704

705 **4.6. Definition of the hurricane season**

706

707 The method based on the seasonality of TC return periods (see 2.2.1) relies on objective criteria and
708 may provide a benchmark for GCMs to reproduce the season dates compared to best-track data. It
709 however depends on the somewhat arbitrary choice of a return period threshold. Nevertheless, TC
710 return periods in the historical runs agree well with IBTrACS even in June and November (Fig. 2),
711 meaning that if it were not for computational constraints, a lower threshold (*e.g.* a 10-year return
712 period) could have been used to more closely match the WMO standard. On the other hand, the
713 projected season shortening would have been more pronounced in such case (Fig. 2), suggesting
714 potential sensitivity of our results to this choice. In addition, the application to other numerical
715 models may yield different dates, complicating any comparison between different studies. As such,
716 it raises the question of reproducibility, which is particularly important for climate projection
717 studies as emphasized by coordinated community efforts such as CMIP or COWCLIP.

718 Fixed, standard dates have the advantage of simplicity and easier reproduction, despite undesired
719 effects in case of shifting future seasons. ASO is the longest sequence of complete months within
720 the W-Hist-Obs, W-Hist-Model and W-RCP8.5 hurricane seasons (Table 3). It lies at the core of the
721 observed season (Fig. 2), therefore providing a relevant testbed for future studies. The sensitivity of
722 some of our key results to the alternative choice of the ASO period was then assessed for this
723 purpose. It was found to be weak, as illustrated by the comparison of Fig. S7, S8 with Fig. 5, 10a,
724 S5ac, suggesting that the conclusions drawn here are not much sensitive to the choice of the exact
725 time period used to represent the hurricane season. The same holds for the season peak. Indeed, the
726 peak of TC activity, around mid-August to mid-September in the model and IBTrACS (Fig. 2),
727 tends to be in phase with the peak of extreme wave activity not only in the eastern Caribbean but
728 also in the mid-latitudes and MDR (Fig. 6d-f, 8cd).

729

730 **4.7. Statistical significance**

731

732 The robustness of wave climate projections in this paper is assessed with various approaches used
733 to compute statistical significance at the standard 5% level (Online Resource 1, sections 1 to 4).
734 According to these, some projected changes were very robust, namely those in mean U_{10} and H_s that
735 appear statistically significant over the whole sub-basin (Fig. 5ab) and most of the hurricane season
736 (Fig. 6a-c). Others are significant at specific locations only, *e.g.* changes in TC numbers, TC-related
737 H_{s0} , or 10-year return levels (Fig. 1, 9bd, 10). Finally, a few changes were not found significant at
738 all, such as exceedance probabilities for extreme H_s thresholds or TC-related H_s (Fig. 6d-f, 9ac).

739 The reader is however advised against systematically dismissing results that are not statistically
740 significant (and taking significant results for granted) because this is not unambiguous evidence of
741 the null hypothesis, as emphasized by Amrhein et al. (2019). The $p < 0.05$ threshold is not only
742 arbitrary, it can erroneously lead to opposed conclusions from studies using very similar data.

743 Additional evidence including physical arguments needs to be considered before drawing
744 conclusions. For example, we relate the non-significant yet sharp peak-season increase in extreme
745 H_s to the concurrent mean H_s decrease, which is smallest and not significant only then (Fig. 6).
746 Although not statistically significant, the increases in MDR TC-related H_s and H_{s1} are consistent
747 with significant increases in H_{s0} and in Cape Verde TC numbers (Fig. 1, 9, S4). This may be
748 particularly relevant for 10-year H_s , for which a conservative and somewhat subjective method had
749 to be adopted (Online Resource 1, section 4). The associated changes may be robust over wider
750 areas than those hatched on Fig. 10 (see also Fig. S5, S8), as suggested by widespread and strong
751 increases in TC regions particularly at the season peak ($\sim+2$ to $+5$ m), and by the similar pattern of
752 projected September increases in TC numbers (Chauvin et al. 2020).

753 **4.8. Implications for future work**

754
755 While TCs make a major contribution to the climatology of extreme wave events in the North
756 Atlantic, mid-latitude storm activity is also a recurrent seasonal source of energy for large wind sea
757 during winter, roughly from November to April. The associated powerful remote swells affect
758 shorelines across the sub-basin and as far south as the eastern Caribbean, thousands of kilometers
759 away where they can cause significant damage (Jury 2018). The smaller islands of the Lesser
760 Antilles are particularly vulnerable to large ocean wave events of both TC and extratropical origin
761 and to the associated storm surge hazard because of their isolation, limited surface and densely
762 populated shorelines, among other factors. Incoming ocean swells are modified by a range of
763 complex processes occurring at both the island and regional scales due to the north-south alignment
764 of islands located in the path of these swells. How future projections of TC-related and mid-latitude
765 extreme wave climate will affect shorelines of small tropical islands such as the Lesser Antilles is a
766 key question from both societal and scientific points of view. The modeling framework presented in
767 this study may then serve as an appropriate framework for downscaled projections over the Lesser
768 Antilles at sub-kilometer-scale resolution in order to address this question. This will be the topic of
769 future research.

770

771 **5. Conclusion**

772

773 High-resolution ensemble atmospheric GCM simulations under present and future RCP8.5 climates
774 were used to drive basin-scale 50-km wave simulations for the Atlantic Ocean and nested 10-km
775 simulations for the TC main development region (MDR) to infer projected future changes in North
776 Atlantic TC-related wave climate. Overall realistic GCM mean low-level circulation and TC
777 characteristics allowed obtaining plausible projections in the associated wave response.

778 Our main conclusions include a large-scale decrease in average wave heights throughout the
779 hurricane season driven by a weaker and poleward-displaced anticyclone, yet concurrent increases
780 in extreme TC-related wave heights in the MDR associated with stronger TC activity around Cape
781 Verde and related changes in wind sea. The largest expected changes in extreme wave heights were
782 however found near the coast of northeastern United States, possibly related to slight poleward
783 displacement of TC activity, and highest during the season peak phase from mid-August to mid-
784 September. Changes were found to be statistically robust in some specific areas.

785

786

787 **Acknowledgements**

788

789 We are grateful to two anonymous reviewers whose detailed and constructive comments greatly
790 helped improve the quality of the original manuscript. We acknowledge L. Aouf for advice with
791 MFWAM calibration/validation, D. Paradis, P. Cantet and R. Osinski for fruitful discussions, and P.-
792

793 C. Dutrieux for help with post-processing algorithms. The altimeter wave data were obtained from
794 the ESA CCI Sea State project. This effort is sponsored by the European Regional Development
795 Fund, Guadeloupe region, grant CR/16-115 C3AF (Changement Climatique et Conséquences sur
796 les Antilles Françaises).

797 **References**

798

799 Alves JHGM (2006) Numerical modeling of ocean swell contributions to the global wind-wave
800 climate. *Ocean Model* 11:98-122.

801 Amrhein V et al (2019) Retire statistical significance. *Nature* 567:305-307. doi:10.1038/d41586-
802 019-00857-9

803 Aouf L (2018) CMEMS quality information document for global ocean waves analysis and
804 forecasting product. CMEMS-GLO-QUID-001_027
805 <http://resources.marine.copernicus.eu/documents/QUID/CMEMS-GLO-QUID-001-027.pdf>

806 Appendini CM, Pedrozo-Acuña A, Meza-Padilla R, Torres-Freyermuth A, Cerezo-Mota R, Lopez-
807 Gonzalez J, Ruiz-Salcines P (2017) On the role of climate change on wind waves generated by
808 tropical cyclones in the Gulf of Mexico. *Coast Eng J* 59:2. doi:10.1142/S0578563417400010.

809 Ardhuin F, Rogers E, Babanin AV, Filipot JF, Magne R, Roland A, van der Westhuysen A,
810 Queffeulou P, Lefevre JM, Aouf L, Collard F (2010) Semiempirical dissipation source functions
811 for ocean waves. Part I: definition, calibration, and validation. *J Phys Oceanogr* 40(9):1917-1941.

812 Batté L, Déqué M (2016) Randomly correcting model errors in the ARPEGE-Climate v6.1
813 component of CNRM-CM: applications for seasonal forecasts. *Geosci Model Dev* 9:2055-2076.
814 doi:10.5194/gmd-9-2055-2016.

815 Bieli M, Camargo SJ, Sobel AH, Evans JL, Hall T (2019a) A global climatology of extratropical
816 transition. Part I: characteristics across basins. *J Clim* 32:3557-3582. doi:10.1175/JCLI-D-17-
817 0518.1.

818 Bieli M, Camargo SJ, Sobel AH, Evans JL, Hall T (2019a) A global climatology of extratropical
819 transition. Part II: statistical performance of the cyclone phase space. *J Clim* 32:3583-3597.
820 doi:10.1175/JCLI-D-18-0052.1.

821 Cantet P, Déqué M, Palany P, Maridet JL (2014) The importance of using a high-resolution model to
822 study the climate change on small islands: The Lesser Antilles case. *Tellus A* 66:24065.
823 doi:10.3402/tellusa.v66.24065.

824 Cantet P, Belmadani A, Chauvin F, Palany P (2020) Projections of tropical cyclone rainfall over
825 land with an Eulerian approach: Case study of three islands in the West Indies. *Int J Climatol* 1–
826 11. doi:10.1002/joc.6760.

827 Camus P, Losada IJ, Izaguirre C, Espejo A, Menéndez M, Pérez J (2017) Statistical wave climate
828 projections for coastal impact assessments. *Earth's Future* 5:918-933. doi:10.1002/2017EF000609.

829 Charles E, Idier D, Delecluse P, Déqué M, Le Cozannet G (2012) Climate change impact on waves
830 in the Bay of Biscay, France. *Ocean Dyn* 62:831-848. doi:10.1007/s10236-012-0534-8.

831 Chauvin F, Royer JF, Déqué D (2006) Response of hurricane-type vortices to global warming as
832 simulated by ARPEGE-Climat at high resolution. *Clim Dyn* 27:377-399.

833 Chauvin F, Pilon R, Palany P, Belmadani A (2020) Future changes in Atlantic hurricanes with the
834 rotated-stretched ARPEGE-Climat at very high resolution. *Clim Dyn* 54:947-972.
835 doi:10.1007/s00382-019-05040-4.

836 Chen X, Ginis I, Hara T (2018) Sensitivity of offshore tropical cyclone wave simulations to spatial
837 resolution in wave models. *J Mar Sci Eng* 6:116. doi:10.3390/jmse6040116.

838 Chen Y, Yu X (2017) Sensitivity of storm wave modeling to wind stress evaluation methods. *J Adv*
839 *Model Earth Sys* 9:893–907. doi:10.1002/2016MS000850

840 Christensen JH, Krishna Kumar K, Aldrian E, An SI, Cavalcanti IFA, de Castro M, Dong W,
841 Goswami P, Hall A, Kanyanga JK, Kitoh A, Kossin J, Lau NC, Renwick J, Stephenson DB, Xie
842 SP, Zhou T (2013) Climate phenomena and their relevance for future regional climate change. In:
843 *Climate change 2013: the physical science basis. Contribution of working group I to the fifth*
844 *assessment report of the intergovernmental panel on climate change* [Stocker, TF, Qin D, Plattner
845 GK, Tignor M, Allen SK, Boschung J, Nauels A, Xia Y, Bex V, Midgley PM (eds.)]. Cambridge
846 University Press, Cambridge, United Kingdom and New York, NY, USA.

847 Church JA, Clark PU, Cazenave A, Gregory JM, Jevrejeva S, Levermann A, Merrifield MA, Milne
848 GA, Nerem RS, Nunn PD, Payne AJ, Pfeffer WT, Stammer D, Unnikrishnan AS (2013) Sea level
849 change. In: *Climate change 2013: the physical science basis. Contribution of working group I to
850 the fifth assessment report of the intergovernmental panel on climate change* [Stocker, TF, Qin D,
851 Plattner GK, Tignor M, Allen SK, Boschung J, Nauels A, Xia Y, Bex V, Midgley PM (eds.)].
852 Cambridge University Press, Cambridge, United Kingdom and New York, NY, USA.

853 Dee DP et al (2011) The ERA-Interim reanalysis: configuration and performance of the data
854 assimilation system. *Q J R Meteorol Soc A* 137:553–597. doi:10.1002/qj.828

855 Déqué M (2007) Frequency of precipitation and temperature extremes over France in an
856 anthropogenic scenario: Model results and statistical correction according to observed values.
857 *Glob Planet Chang* 57:16–26.

858 Diro GT, Giorgi F, Fuentes-Franco R, Walsh KJE, Giuliani G, Coppola E (2014) Tropical cyclones
859 in a regional climate change projection with RegCM4 over the CORDEX Central America
860 domain. *Climatic Change* 125:79-94. doi:10.1007/s10584-014-1155-7

861 Dodet G et al (2020) The Sea State CCI dataset v1: towards a sea state climate data record based on
862 satellite observations. *Earth Sys Sci Data* 12:1929-1951. doi:10.5194/essd-12-1929-2020.

863 Emanuel KA (2013) Downscaling CMIP5 climate models shows increased tropical cyclone activity
864 over the 21st century. *Proc Natl Acad Sci USA* 110:12219–12224. doi:10.1073/pnas.1301293110.

865 Fan Y, Held I M, Lin SJ, Wang XL (2013) Ocean warming effect on surface gravity wave climate
866 change for the end of the twenty-first century. *J Clim* 26:6046-6066.

867 Fan Y, Lin SJ, Griffies SM, Hemer MA (2014) Simulated global swell and wind-sea climate and
868 their responses to anthropogenic climate change at the end of the twenty-first century. *J Clim*
869 27:3516-3536.

870 Gastineau G, Li L, Le Treut H (2009) The Hadley and Walker circulation changes in global
871 warming conditions described by idealized atmospheric simulations. *J Clim* 22:3993–4013.
872 doi:10.1175/2009JCLI2794.1.

873 Guo L, Perrie W, Long Z, Toulany B, Sheng J (2015) The impacts of climate change on the autumn
874 North Atlantic wave climate. *Atmosphere-Ocean* 53:491-509.
875 doi:10.1080/07055900.2015.1103697

876 Harris DL (1963) Characteristics of the hurricane storm surge. Tech Rep 48, US Weather Bureau,
877 Department of Commerce, Washington, DC.

878 Hasselmann S, Brüning C, Hasselmann K, Heimbach P (1996) An improved algorithm for retrieval
879 of ocean wave spectra from synthetic aperture radar image spectra. *J Geophys Res* 101:16615-
880 16629.

881 Hemer MA, Katzfey J, Trenham CE (2013a) Global dynamical projections of surface ocean wave
882 climate for a future high greenhouse gas emission scenario. *Ocean Model* 70:221-245.
883 doi:10.1016/j.ocemod.2012.09.008.

884 Hemer M, Fan Y, Mori N, Semedo A, Wang X (2013b) Projected changes in wave climate from a
885 multi-model ensemble. *Nature Clim Change*. doi:10.1038/nclimate1791.

886 Hemer M, Wang W, Charles E, Hegermiller C & COWCLIP contributors (2014) Report of the 2014
887 meeting for the WCRP-JCOMM Coordinated Global Wave Climate Projections (COWCLIP),
888 WMO 2014.

889 Hemer MA, Trenham CE (2016) Evaluation of a CMIP5 derived dynamical global wind wave
890 climate model ensemble. *Ocean Model* 103:190-203. doi:10.1016/j.ocemod.2015.10.009.

891 Hemer M, Wang X, Webb A & COWCLIP contributors (2018) Report of the 2018 meeting for the
892 WCRP-JCOMM Coordinated Global Wave Climate Projections (COWCLIP), WMO 2018.

893 Hersbach H et al (2020) The ERA5 global reanalysis. *Q J R Meteorol Soc*. doi:10.1002/qj.3803

894 Johanson CM, Fu Q (2009) Hadley cell widening: model simulations versus observations. *J Clim*
895 22:2713–2725. doi:10.1175/2008JCLI2620.1.

896 Jullien S, Marchesiello P, Menkes CE, Lefèvre J, Jourdain NC, Samson G, Lengaigne M (2014)
897 Ocean feedback to tropical cyclones: climatology and processes. *Clim Dyn* 43:2831-2854.
898 doi:10.1007/s00382-014-2096-6.

899 Jury MR (2018) Characteristics and meteorology of Atlantic swells reaching the Caribbean. *J*
900 *Coastal Res* 34:400-412. doi:10.2112/JCOASTRES-D-17-00029.1.

901 Kar-Man Chang E (2018) CMIP5 projected change in Northern Hemisphere winter cyclones with
902 associated extreme winds. *J Clim* 31:6527–6542.

903 Kishimoto R, Shimura T, Mori N, Mase H (2017) Statistical modeling of global mean wave height
904 considering principal component analysis of sea level pressures and its application to future wave
905 height projection. *Hydrol Res Lett* 11:51-57. doi:10.3178/HRL.11.51.

906 Knapp KR, Kruk MC, Levinson DH, Diamond HJ, Neumann CJ (2010) The International Best
907 Track Archive for Climate Stewardship (IBTrACS): unifying tropical cyclone data. *Bull Amer*
908 *Meteorol Soc* 91:363-376. doi:10.1175/2009BAMS2755.1.

909 Komar PD (1998) Beach processes and sedimentation. Prentice-Hall, Upper Saddle River, NJ, 2nd
910 edition, 546 pp., ISBN 0-13754-938-5.

911 Krien Y, Arnaud G, Cécé R, Ruf C, Belmadani A, Khan J, Bernard D, Islam AKMS, Durand F,
912 Testut L, Palany P, Zahibo N (2018) Can we improve parametric cyclonic wind fields using recent
913 satellite remote sensing data? *Remote Sens* 10:1963. doi:10.3390/rs10121963.

914 Laugel A, Menendez M, Benoit M, Mattarolo G, Méndez F (2014) Wave climate projections along
915 the French coastline: dynamical versus statistical downscaling methods. *Ocean Model* 84:35-50.
916 doi:10.1016/j.ocemod.2014.09.002.

917 Lemos G, Menendez M, Semedo A, Camus P, Hemer M, Dobrynin M, Miranda PMA (2020) On the
918 need of bias correction methods for wave climate projections. *Glob Planet Chang* 186.
919 doi:10.1016/j.gloplacha.2019.103109.

920 Moon I, Hara T, Ginis I, Belcher SE, Tolman HL (2004) Effect of surface waves on air-sea
921 momentum exchange: I. Effect of mature and growing seas. *J Atmos Sci* 61(19):2321–2333.

922 Mori N, Yasuda T, Mase H, Tom T, Oku Y (2010) Projection of extreme wave climate change under
923 global warming. *Hydrol Res Lett* 4:15-19. doi:10.3178/HRL.4.15.

924 Mori N, Shimura T, Yasuda T, Mase H (2013) Multi-model climate projections of ocean surface
925 variables under different climate scenarios – Future change of waves, sea level and wind. *Ocean*
926 *Eng* 71:122-129. doi:10.1016/j.oceaneng.2013.02.016.

927 Morim J, Hemer M, Cartwright N, Strauss D, Andutta F (2018) On the concordance of 21st century
928 wind-wave climate projections. *Global Planet Change* 167:160-171.

929 Morim J, Hemer M, Wang XL, Cartwright N, Trenham C, Semedo A, Young I, Bricheno L, Camus
930 P, Casas-Prat M, Erikson L, Mentaschi L, Mori N, Shimura T, Timmermans B, Aarnes O, Breivik
931 O, Behrens A, Dobrynin M, Menendez M, Staneva J, Wehner M, Wolf J, Kamranzad B, Webb A,
932 Stopa J, Andutta F (2019) Robustness and uncertainties in global multivariate wind-wave climate
933 projections. *Nature Clim Change*. doi:10.1038/s41558-019-0542-5.

934 Murakami H, Mizuta R, Shindo E (2012) Future changes in tropical cyclone activity projected by
935 multi-physics and multi-SST ensemble experiments using the 60-km-mesh MRI-AGCM. *Clim*
936 *Dyn* 39:2569–2584. doi:10.1007/s00382-011-1223-x.

937 Perez J, Menendez M, Losada IJ (2017) GOW2: A global wave hindcast for coastal applications.
938 *Coastal Eng* 124:1-11. doi:10.1016/j.coastaleng.2017.03.005.

939 Piolle JF, Dodet G, Ash E (2020) ESA Sea State Climate Change Initiative: Product user guide,
940 version 1.0. [http://dap.ceda.ac.uk/thredds/fileServer/neodc/esacci/sea_state/docs/v1.1/
941 Sea State cci PUG v1.0-signed.pdf](http://dap.ceda.ac.uk/thredds/fileServer/neodc/esacci/sea_state/docs/v1.1/Sea_State_cci_PUG_v1.0-signed.pdf)

942 Powell, MD, Vickery PJ, Reinhold TA (2003) Reduced drag coefficient for high wind speeds in
943 tropical cyclones. *Nature* 422(6929):279–283.

944 Rappaport EN (2014) Fatalities in the United States from Atlantic tropical cyclones: new data and
945 interpretation. *Bull Amer Meteorol Soc* 95:341-346. doi:10.1175/BAMS-D-12-00074.1.

946 Rayner NA, Parker DE, Horton EB, Folland CK, Alexander LV, Rowell DP, Kent EC, Kaplan A
947 (2003) Global analyses of sea surface temperature, sea ice, and night marine air temperature since
948 the late nineteenth century. *J Geophys Res* 108:4407. doi:10.1029/2002JD002670.

949 Rey T, Leone F, Candela T, Belmadani A, Palany P, Krien Y, Cécé R, Gherardi M, Péroche M,
950 Zahibo N (2019) Coastal processes and influence on damage to urban structures during Hurricane
951 Irma (St-Martin & St-Barthélemy, French West Indies). *J Mar Sci Eng* 7:215.
952 doi:10.3390/jmse7070215.

953 Roberts MJ, et al (2020a) Impact of model resolution on tropical cyclone simulation using the
954 HighResMIP–PRIMAVERA multimodel ensemble. *J Clim* 33:2557-2583. doi:10.1175/JCLI-D-19-
955 0639.1.

956 Roberts MJ, et al (2020b) Projected future changes in tropical cyclones using the CMIP6
957 HighResMIP multi-model ensemble. *Geophys Res Lett* 47:e2020GL088662.
958 doi:10.1029/2020GL088662.

959 Roehrig R, et al (2020) The CNRM global atmosphere model ARPEGE-Climat 6.3: Description and
960 evaluation. *J Adv Model Earth Sys* 12:e2020MS002075. doi:10.1029/2020MS002075.

961 Scoccimarro E, Gualdi S, Bellucci A, Sanna A, Fogli PG, Manzini E, Vichi M, Oddo P, Navarra A
962 (2011) Effects of tropical cyclones on ocean heat transport in a high-resolution coupled general
963 circulation model. *J Clim* 24:4368-4384. doi:10.1175/2011jcli4104.1.

964 Semedo A, Sušelj K, Rutgersson A, Sterl A (2011) A global view on the wind sea and swell climate
965 and variability from ERA-40. *J Clim* 24:1461-1479. doi: 10.1175/2010JCLI3718.1.

966 Semedo A, Weisse R, Behrens A, Sterl A, Bengtsson L, Günther H (2013) Projection of global wave
967 climate change toward the end of the twenty-first century. *J Clim* 26:8269-8288.
968 doi:10.1175/JCLI-D-12-00658.1.

969 Semedo A, Dobrynin M, Lemos G, Behrens A, Staneva J, De Vries H, Sterl A, Bidlot JR, Miranda
970 PMA, Murawski J (2018) CMIP5-derived single-forcing, single-model, and single-scenario wind-
971 wave climate ensemble: configuration and performance evaluation. *J Mar Sci Eng* 6:90.
972 doi:10.3390/jmse6030090.

973 Shimura T, Mori N, Mase H (2015) Future projections of extreme ocean wave climates and the
974 relation to tropical cyclones: ensemble experiments of MRI-AGCM3.2H. *J Clim* 28:9838-9856.

975 Stockdon HF, Holman RA, Howd PA, Sallenger AH (2006) Empirical parameterization of setup,
976 swash, and runup. *Coastal Eng* 53:573-588.

977 Stockdon HF, Thompson DM, Plant NG, Long JW (2014) Evaluation of wave runup predictions
978 from numerical and parametric models. *Coastal Eng* 92:1-11.

979 Stopa JE (2018) Wind forcing calibration and wave hindcast comparison using multiple reanalysis
980 and merged satellite wind datasets. *Ocean Model* 127:55-69. doi:10.1016/j.ocemod.2018.04.008.

981 Timmermans B, Stone D, Wehner M, Krishnan H (2017) Impact of tropical cyclones on modeled
982 extreme wind-wave climate. *Geophys Res Lett* 44:1393-1401. doi:10.1002/2016GL071681.

983 Timmermans BW, Gommenginger CP, Dodet G, Bidlot JR (2020) Global wave height trends and
984 variability from new multimission satellite altimeter products, reanalyses, and wave buoys.
985 *Geophys Res Lett* 47. doi:10.1029/2019GL086880.

986 Voldoire A, et al (2019) Evaluation of CMIP6 DECK experiments with CNRM-CM6-1. *J Adv*
987 *Model Earth Sys* 11(7):2177-2213.

988 Vousdoukas MI, Mentaschi L, Voukouvalas E, Verlaan M, Jevrejeva S, Jackson LP, Feyen L (2018a)
989 Global probabilistic projections of extreme sea levels show intensification of coastal flood
990 hazard. *Nature Comm* 9:2360. doi:10.1038/s41467-018-04692-w.

991 Vousdoukas MI, Mentaschi L, Voukouvalas E, Bianchi A, Dottori F, Feyen L (2018b) Climatic and
992 socioeconomic controls of future coastal flood risk in Europe. *Nature Clim Change* 8:776-780.
993 doi:10.1038/s41558-018-0260-4.

994 WAMDI Group (1988) The WAM model: a third-generation ocean wave prediction model. *J Phys*
995 *Oceanogr* 18:1775-1810.

996 Wang XL, Feng Y, Swail VR (2014) Changes in global ocean wave heights as projected using
997 multimodel CMIP5 simulations. *Geophys Res Lett* 41:1026-1034. doi:10.1002/2013GL058650.
998 Wang XL, Feng Y, Swail VR (2015) Climate change signal and uncertainty in CMIP5-based
999 projections of global ocean surface wave heights. *J Geophys Res Oceans* 120:3859-3871.
1000 doi:10.1002/2015JC010699.
1001 Webb A, Shimura T, Mori N (2018) A high-resolution future wave climate projection for the coastal
1002 northwestern Atlantic. *J Japan Soc Civil Eng, Ser B2 (Coastal Eng)*, 74:1345–1350.
1003 doi:10.2208/kaigan.74.I_1345.
1004 Wehner M, Prabhat, Reed KA, Stone D, Collins WD, Bacmeister J (2015) Resolution dependence
1005 of future tropical cyclone projections of CAM5.1 in the U.S. CLIVAR hurricane working group
1006 idealized configurations. *J Clim* 28:3905–3925. doi:10.1175/JCLI-D-14-00311.1.
1007 World Meteorological Organization (2014) Atlas of mortality and economic losses from weather,
1008 climate and water extremes (1970-2012). WMO-No. 1123.
1009 Zelinsky DA (2019) Hurricane Lorenzo. Tropical Cyclone Report, National Hurricane Center,
1010 Miami, FL, USA. Available online: https://www.nhc.noaa.gov/data/tcr/AL132019_Lorenzo.pdf
1011 (accessed on 1 June 2020).

Climate Experiment	Monthly SST Forcing	Time Slice (Chauvin et al 2020)	Time Slice (this study)	Number of Ensemble Members
Hist-Obs	HadISST1	1965-2014	1984-2013	5
Hist-Model	CNRM-CM5, historical, corrected	1965-2013	1984-2013	5
RCP8.5	CNRM-CM5, RCP8.5, corrected	2031-2080	2051-2080	5

1012 **Table 1.** Summary of the ARPEGE-Climat simulations used to drive the wave models.

1013

Numerical Model	Geographical Domain	Horizontal Resolution	Boundary Forcing
ARPEGE-Climat	Global	Variable (Chauvin et al. 2020, their Fig. 1) Atlantic: TC regions 14-30 km (Gulf of Mexico ~35 km), subpolar regions 30-60 km, South Atlantic 30-100 km	None
MFWAM05	Atlantic 59.5°S-70°N/99°W-21°E	50 km	None
MFWAM01	MDR 5°N-28°N/75°W-10°W	10 km	MFWAM05 3-hourly wave spectra

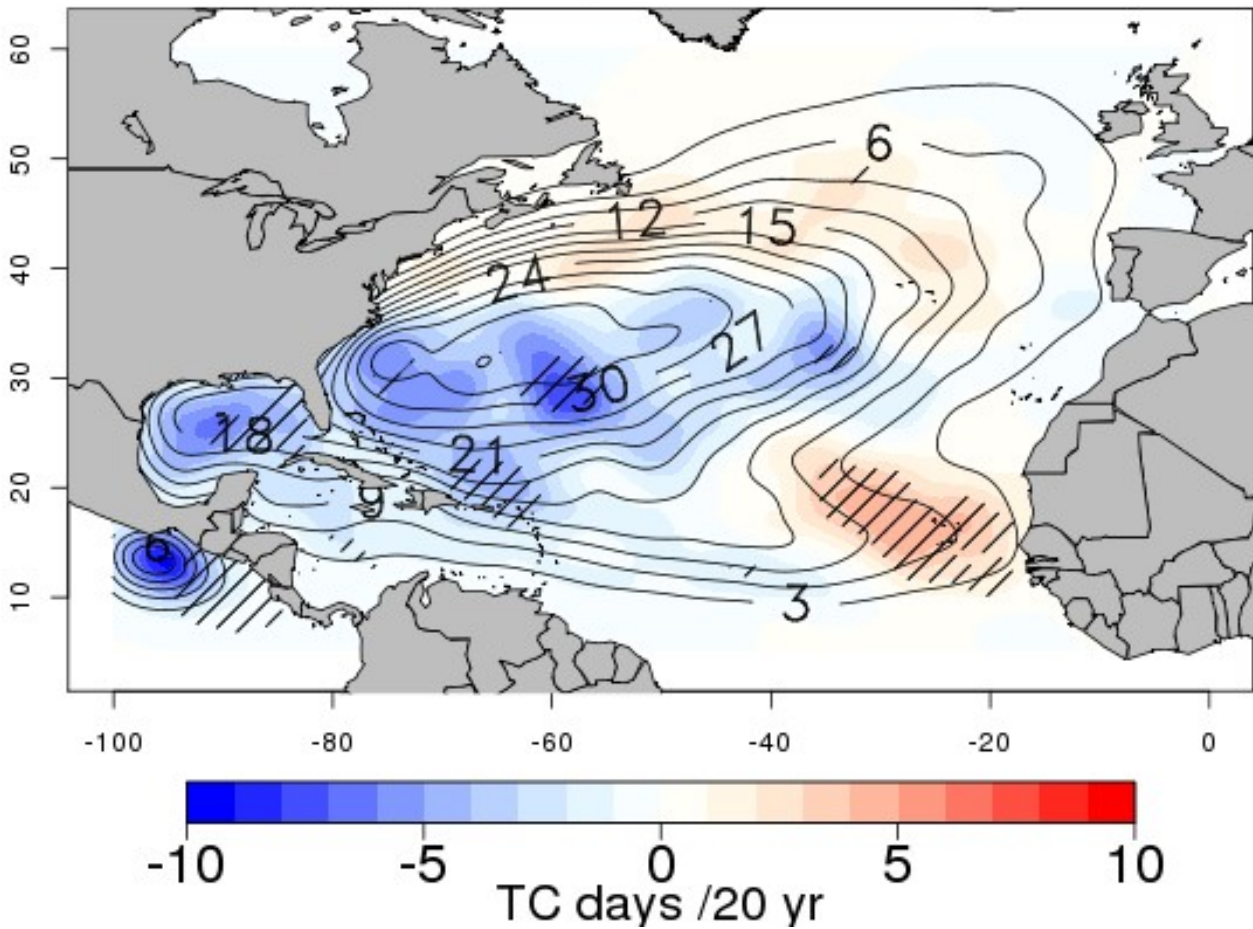
1014 **Table 2.** Summary of the horizontal grids considered for ARPEGE-Climat and for the MFWAM nested domains.

1015

Climate Experiment	6-hourly ARPEGE-Climat Wind Forcing	30-Year Time Slice	Period Simulated Each Year	Number of Ensemble Members	Number of Simulated Hurricane Seasons
W-Hist-Obs	Hist-Obs	1984-2013	July 9 - November 9	5	150
W-Hist-Model	Hist-Model	1984-2013	July 6 - November 10	5	150
W-RCP8.5	RCP8.5	2051-2080	July 20 - November 3	5	150

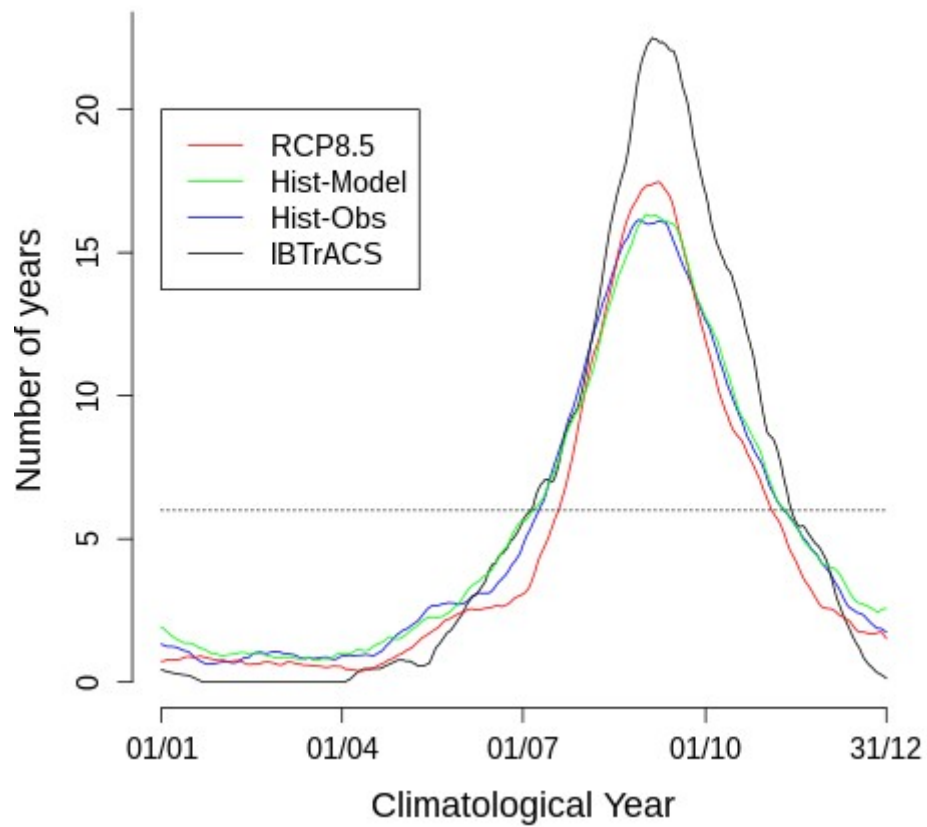
1016 **Table 3.** Summary of the MFWAM wave climate simulations. The information provided applies to both MFWAM05
1017 and MFWAM01.

2031-2080: Change in TC days ARPEGE



1018
1019 **Fig. 1.** Projected changes in the frequency of TC days between RCP8.5 (2031-2080) and Hist-Model (1965-2013).
1020 Values are expressed as a distance-weighted number of TC days per 20 years by $5^\circ \times 5^\circ$ square. Gaussian diffusion has
1021 been applied. Hist-Model frequency of TC days is overlaid as black contours. Hatchings are for the 5% significance
1022 level (Online Resource 1, section 1). Adapted with permission from Chauvin et al. (2020).

Nb of TC years in ARPEGE and IBTRaCS



1023
1024 **Fig. 2.** Ensemble mean number of years with a TC day for each calendar day from RCP8.5 (2051-2080, red), Hist-
1025 Model (1984-2013, green), Hist-Obs (1984-2013, blue), and IBTrACS (1984-2013, black). The horizontal dotted line
1026 indicates the threshold used to define the hurricane season (6 years out of 30 *i.e.* every 5 years). A 30-day moving
1027 average was applied to filter out high-frequency noise.

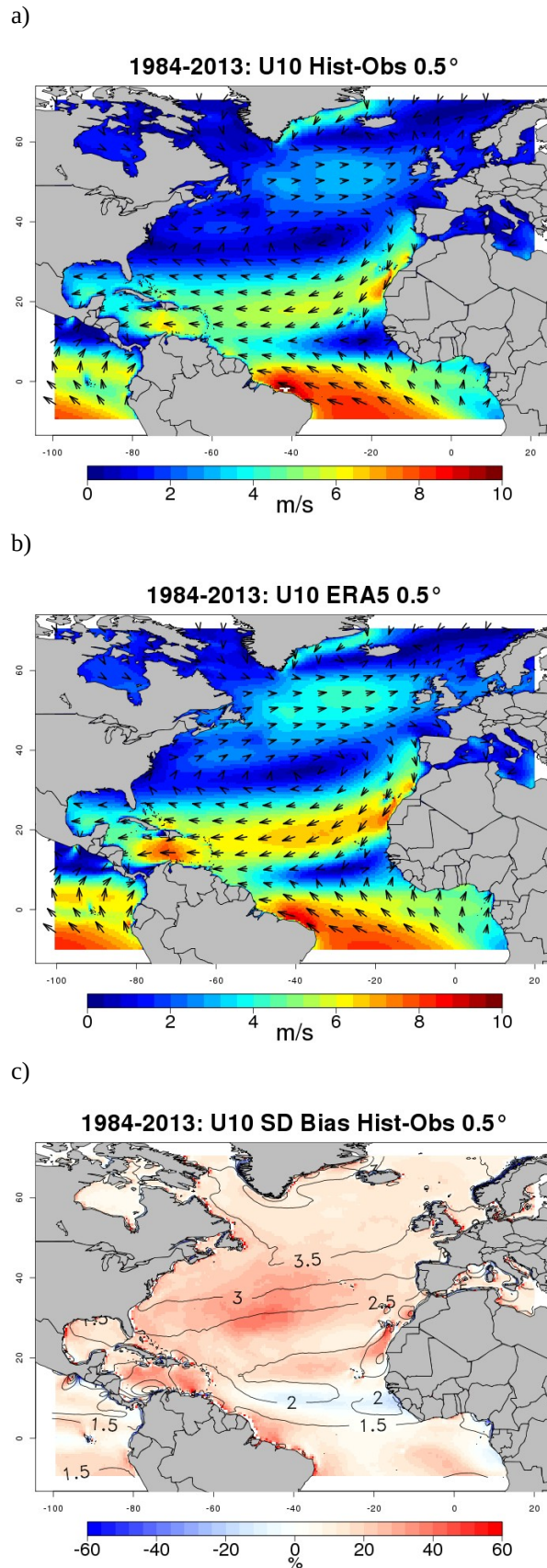


Fig. 3. (a,b) Mean present-climate (1984-2013) hurricane-season surface winds (arrows) and wind speed U_{10} (shading, m.s^{-1}) in a) Hist-Obs and b) ERA5. c) Relative differences in the standard deviation of present-climate hurricane-season U_{10} between Hist-Obs and ERA5 (shading, %), with ERA5 values overlaid as black contours (m.s^{-1}). All the data have been interpolated onto a 0.5° grid and are masked over land.

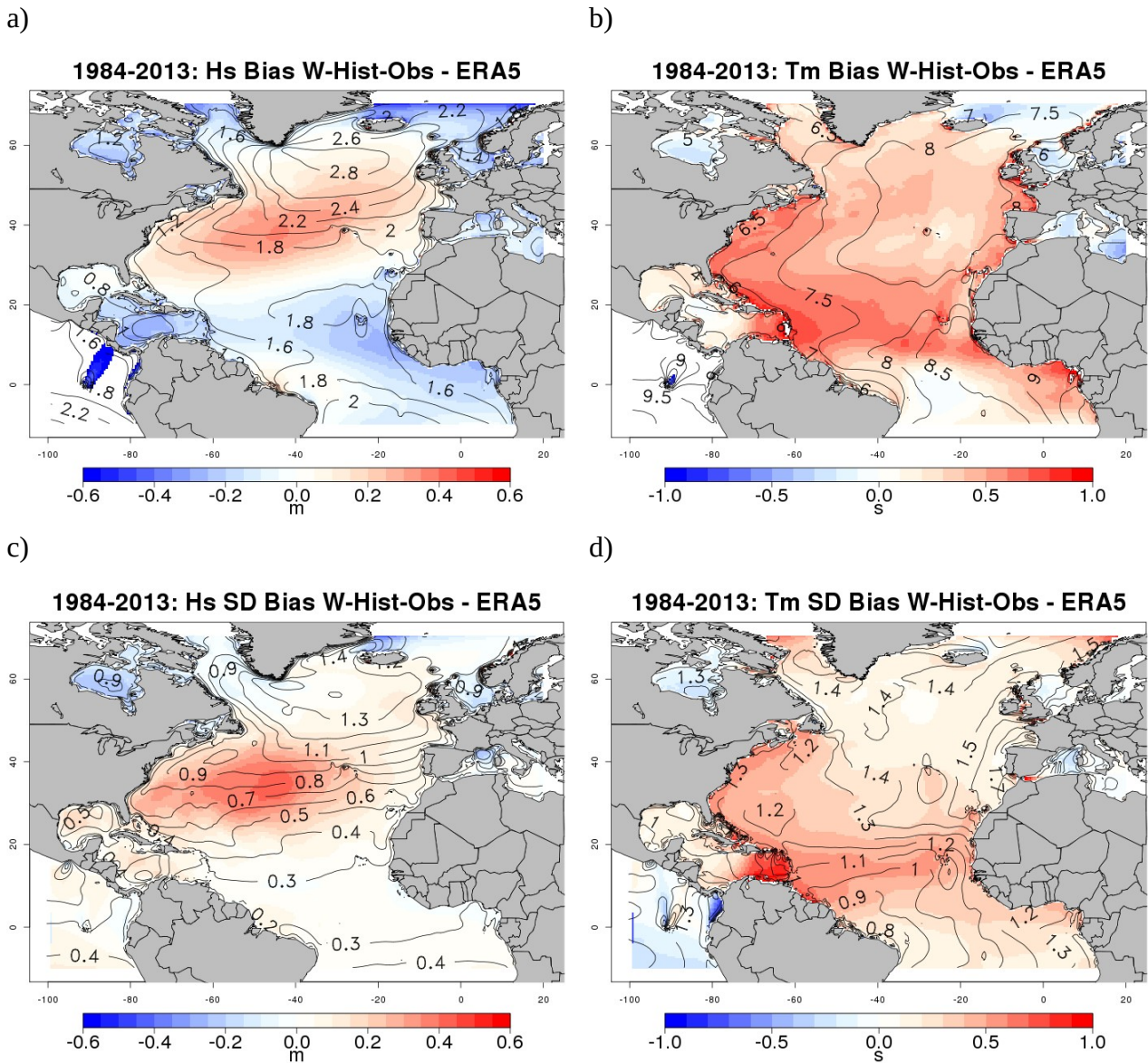


Fig. 4. Differences in the (a,b) mean and (c,d) standard deviation of present-climate (1984-2013) hurricane-season (a,c) significant wave height H_s (m) and (b,d) mean wave period T_m (s) between MFWAM05 W-Hist-Obs and ERA5 (shading), with ERA5 values overlaid as black contours. The ERA5 data have been interpolated onto a 0.5° grid. Differences exceeding ± 0.6 m or ± 1.0 s are masked.

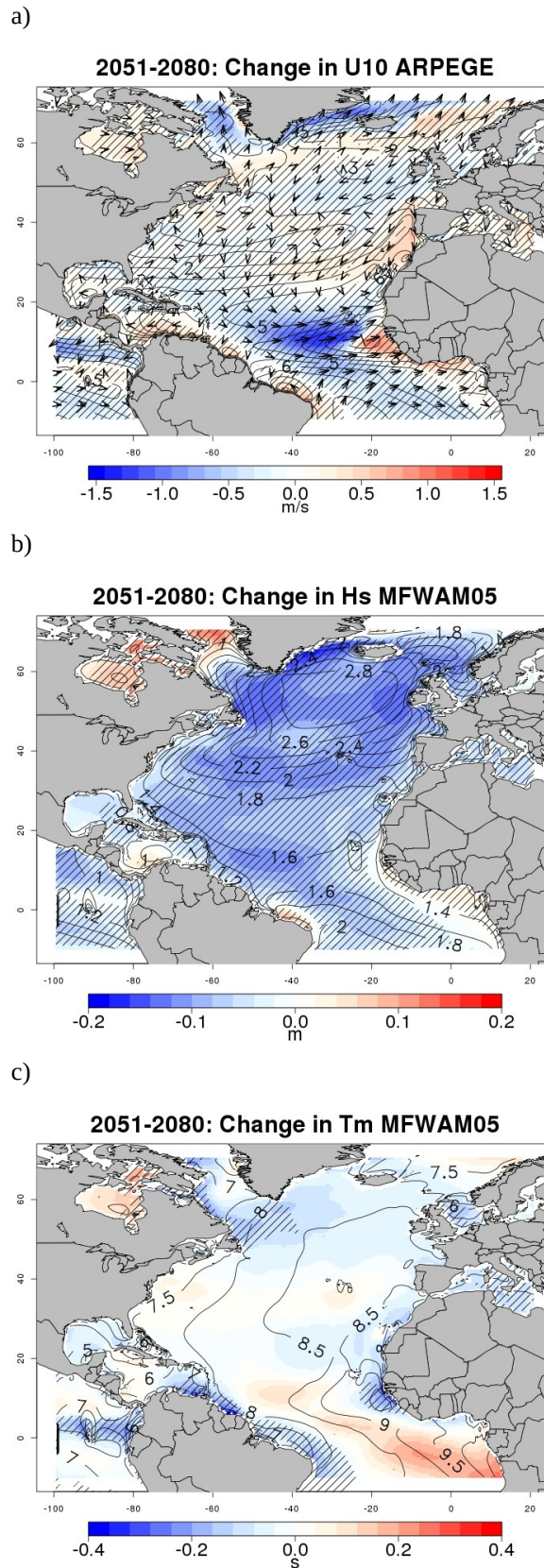


Fig. 5. Projected changes in hurricane-season mean a) surface winds (arrows) and wind speed U_{10} (shading, $\text{m}\cdot\text{s}^{-1}$) from ARPEGE-Climat, b) significant wave height H_s (m) and c) mean wave period T_m (s) from MFWAM05 between W-RCP8.5 (2051-2080) and W-Hist-Model (1984-2013). W-Hist-Model values for U_{10} , H_s , and T_m are overlaid as black contours. Hatchings are for the 5% significance level (Online Resource 1, section 2). ARPEGE-Climat data are masked over land. The arrows on (a) are for the difference between W-RCP8.5 and W-Hist-Model wind vectors.

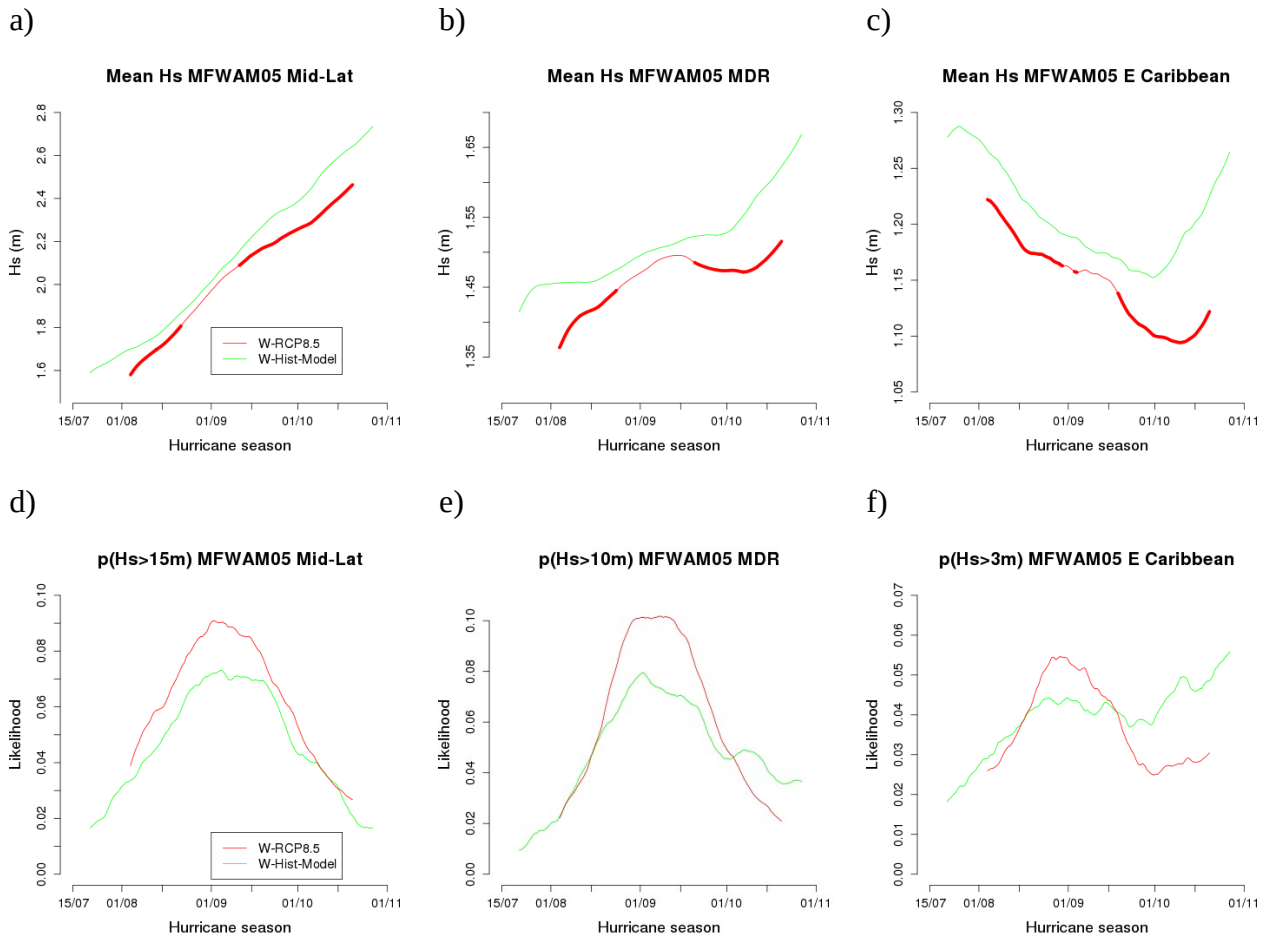


Fig. 6. (a-c) Mean significant wave height H_s (m) for each calendar 3-hourly time step during the hurricane season from MFWAM05 W-RCP8.5 (2051-2080, red) and W-Hist-Model (1984-2013, green) simulations over the a) mid-latitudes (30-50°N, 20-80°W), b) MDR (5-28°N, 10-75°W), and c) eastern Caribbean (11.7-19°N, 59-64°W). (d-f) Ensemble mean likelihood (over 30 years) that the maximum significant wave height H_s over d) the mid-latitudes exceeds 15 m, e) the MDR exceeds 10 m, and f) the eastern Caribbean exceeds 3 m for each calendar 3-hourly time step during the hurricane season from MFWAM05 W-RCP8.5 (red) and W-Hist-Model (green) simulations. Thick red lines are for differences W-RCP8.5 minus W-Hist-Model significant at the 5% level (Online Resource 1, sections 2 and 4). A 30-day moving average was applied to filter out high-frequency noise.

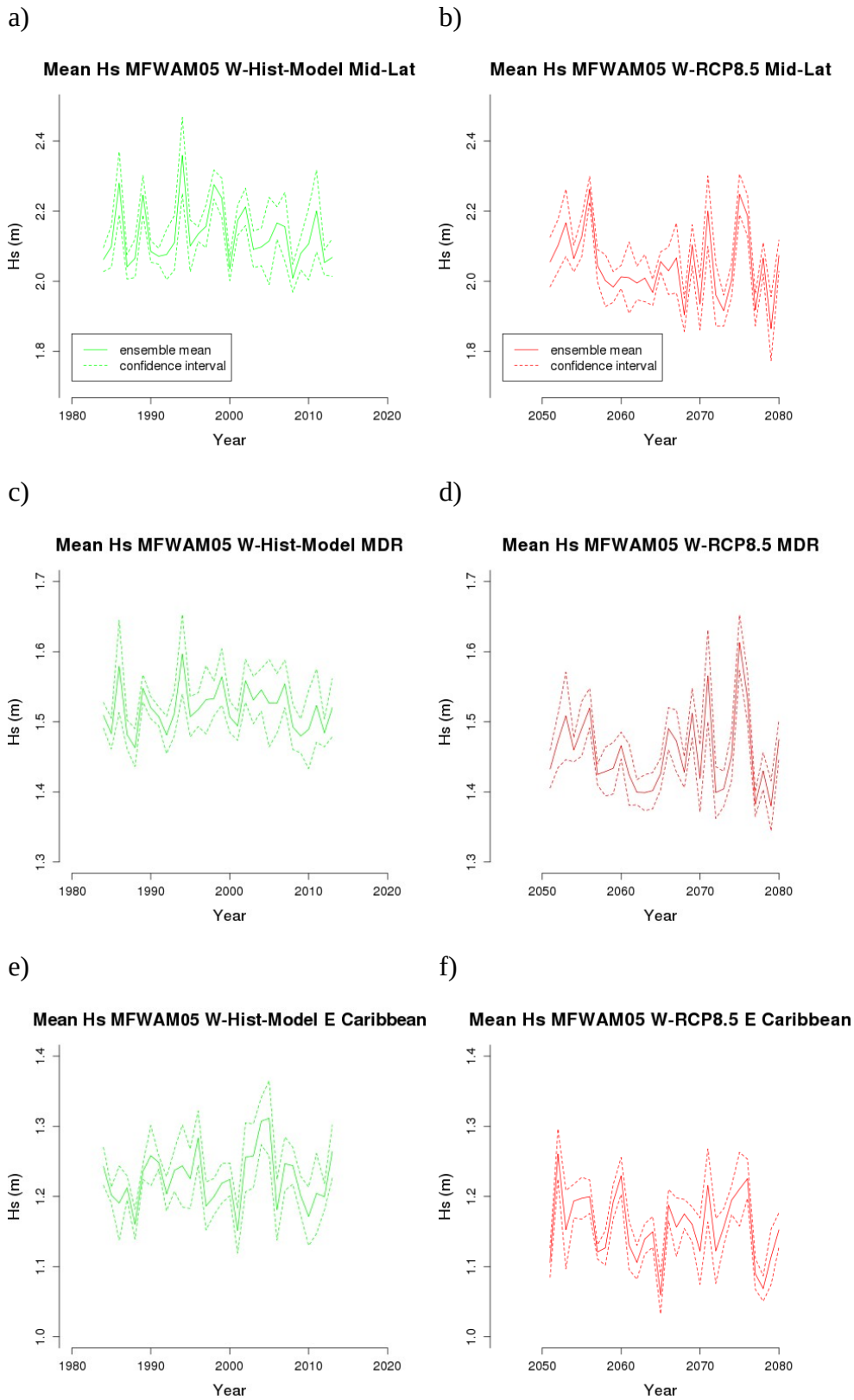


Fig. 7. Annual time series of hurricane-season mean significant wave height H_s (m) from MFWAM05 (a,c,e) W-Hist-Model (1984-2013, solid green line) and (b,d,f) W-RCP8.5 simulations (2051-2080, solid red line) over the (a,b) mid-latitudes, (c,d) MDR, and (e,f) eastern Caribbean. The dashed green/red lines indicate the associated confidence intervals (Online Resource 1, section 5).

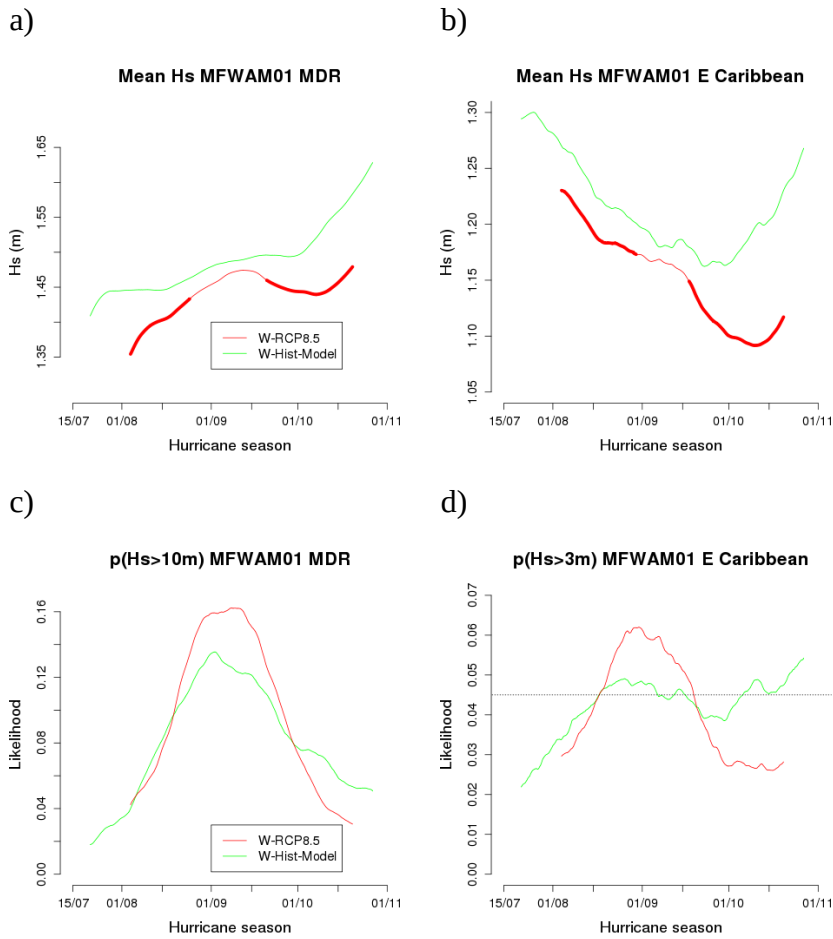


Fig. 8. (a,b) same as Fig. 6bc and (c,d) same as Fig. 6ef, except from MFWAM01. The horizontal dotted line on (d) indicates the threshold used to define the hurricane season peak phase (4.5% *i.e.* 1.35 years).

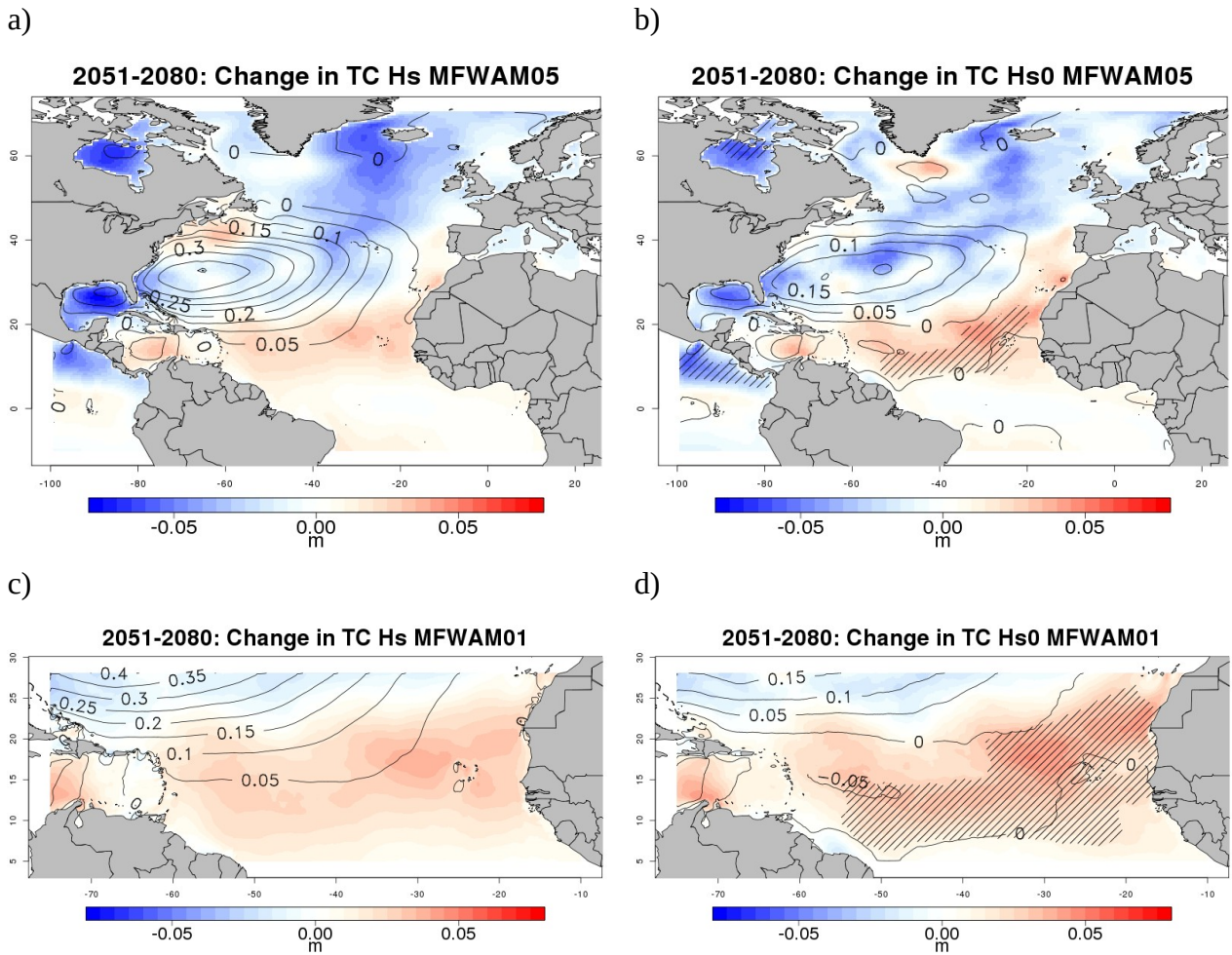


Fig. 9. Projected changes in mean TC-related (a,c) significant wave height H_s (m) and (b,d) significant height of wind waves H_{s0} (m) from (a,b) MFWAM05 and (c,d) MFWAM01 between W-RCP8.5 (2051-2080) and W-Hist-Model (1984-2013). W-Hist-Model values for H_s and H_{s0} are overlaid as black contours. Hatchings are for the 5% significance level.

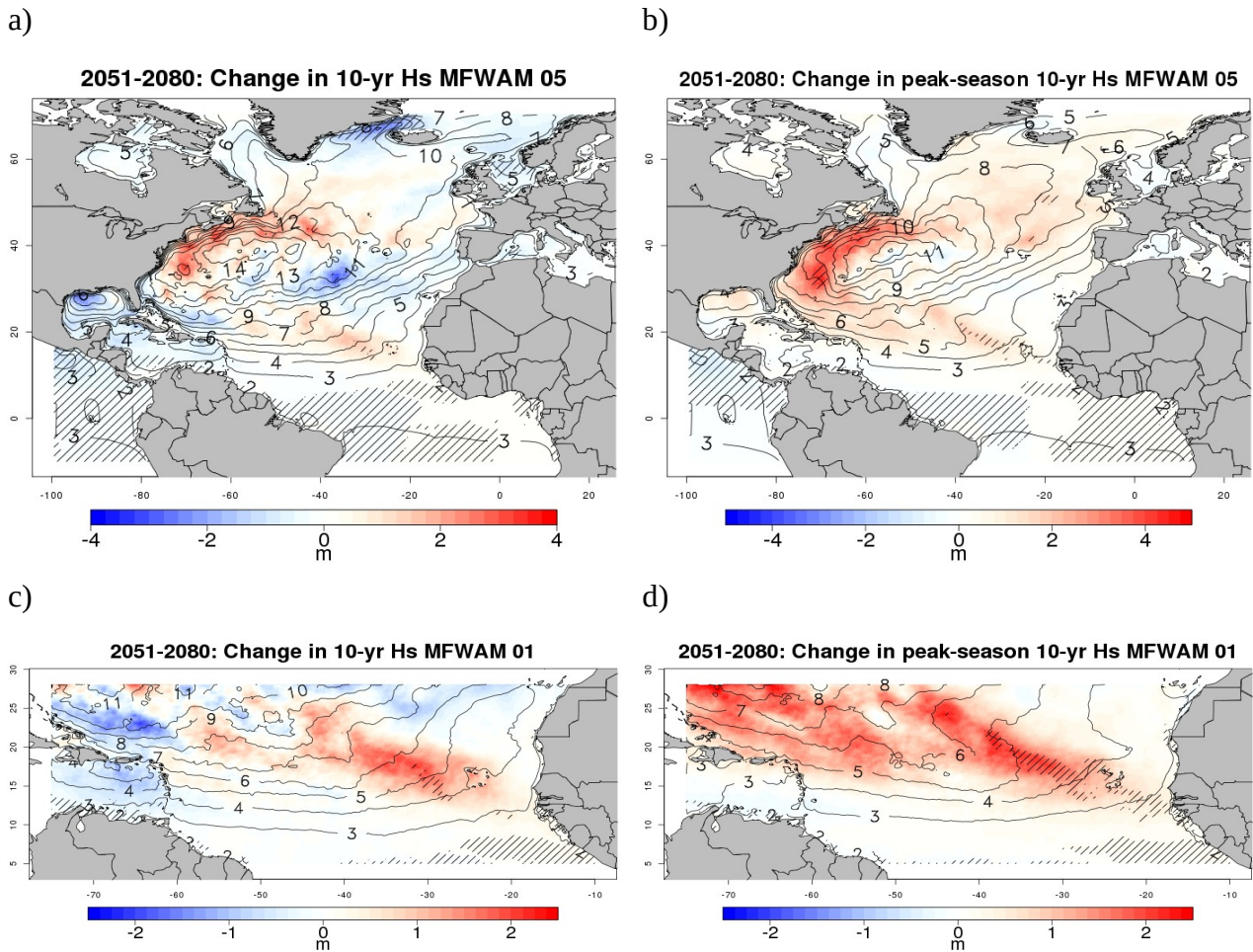


Fig. 10. Projected changes in 10-year TC-related significant wave height H_s (m) from (a,b) MFWAM05 and (c,d) MFWAM01 during (a,c) the hurricane season and (b,d) its peak phase between W-RCP8.5 (2051-2080) and W-Hist-Model (1984-2013). W-Hist-Model values are overlaid as black contours. Hatchings are for the 5% significance level.

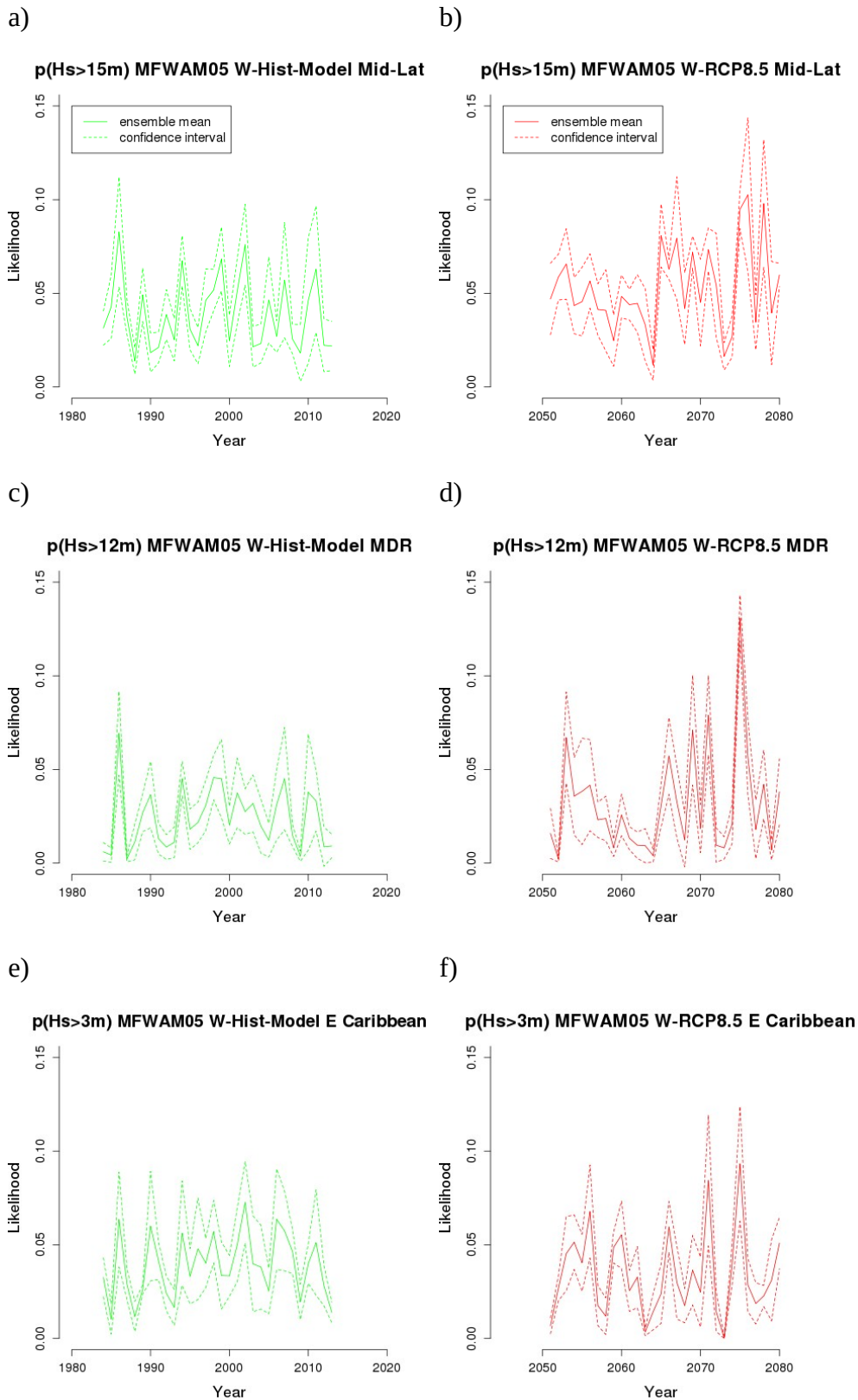


Fig. 11. Annual time series of the likelihood (over the hurricane season) that the maximum significant wave height H_s from MFWAM05 (a,c,e) W-Hist-Model (1984-2013, solid green line) and (b,d,f) W-RCP8.5 simulations (2051-2080, solid red line) over (a,b) the mid-latitudes exceeds 15 m, (c,d) the MDR exceeds 12 m, and (e,f) the eastern Caribbean exceeds 3 m. The dashed green/red lines indicate the associated confidence intervals (Online Resource 1, section 5).

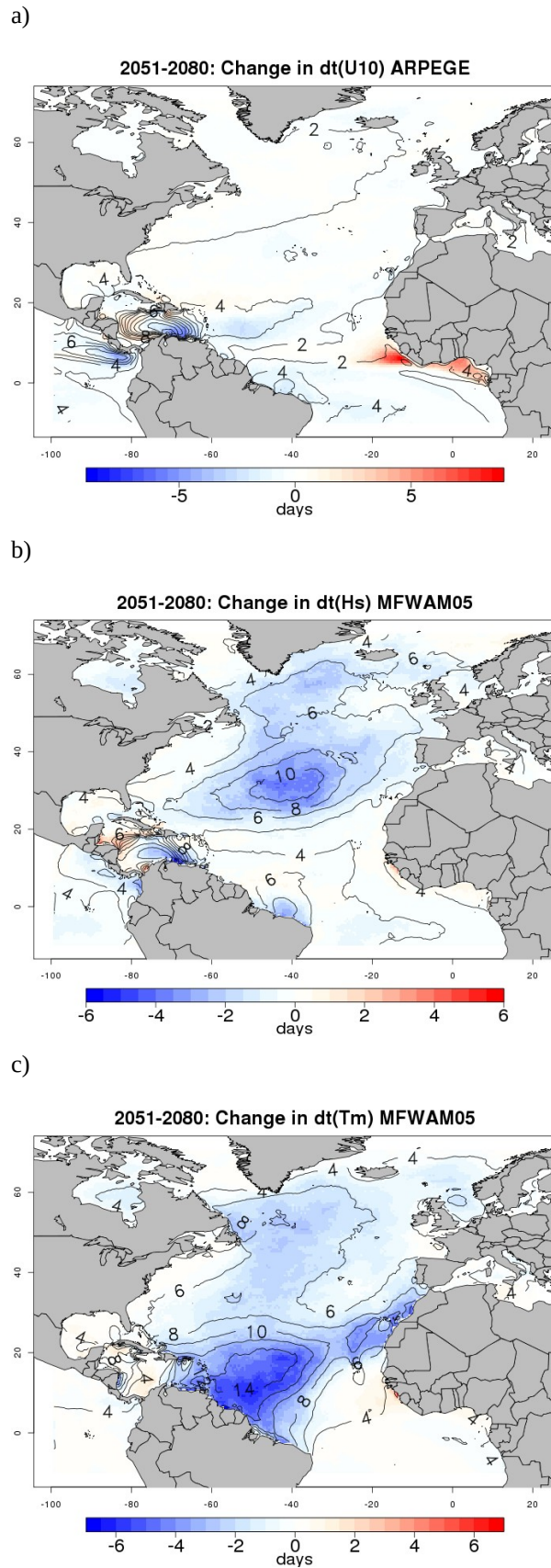


Fig. S1. Projected changes in decorrelation time scales (days) for hurricane-season a) surface wind speed U_{10} from ARPEGE-Climat, b) significant wave height H_s and c) mean wave period T_m from MFWAM05 between W-RCP8.5 (2051-2080) and W-Hist-Model (1984-2013). W-Hist-Model values are overlaid as black contours. ARPEGE-Climat data are masked over land.

1984-2013: U10 Bias Hist-Obs 0.5°

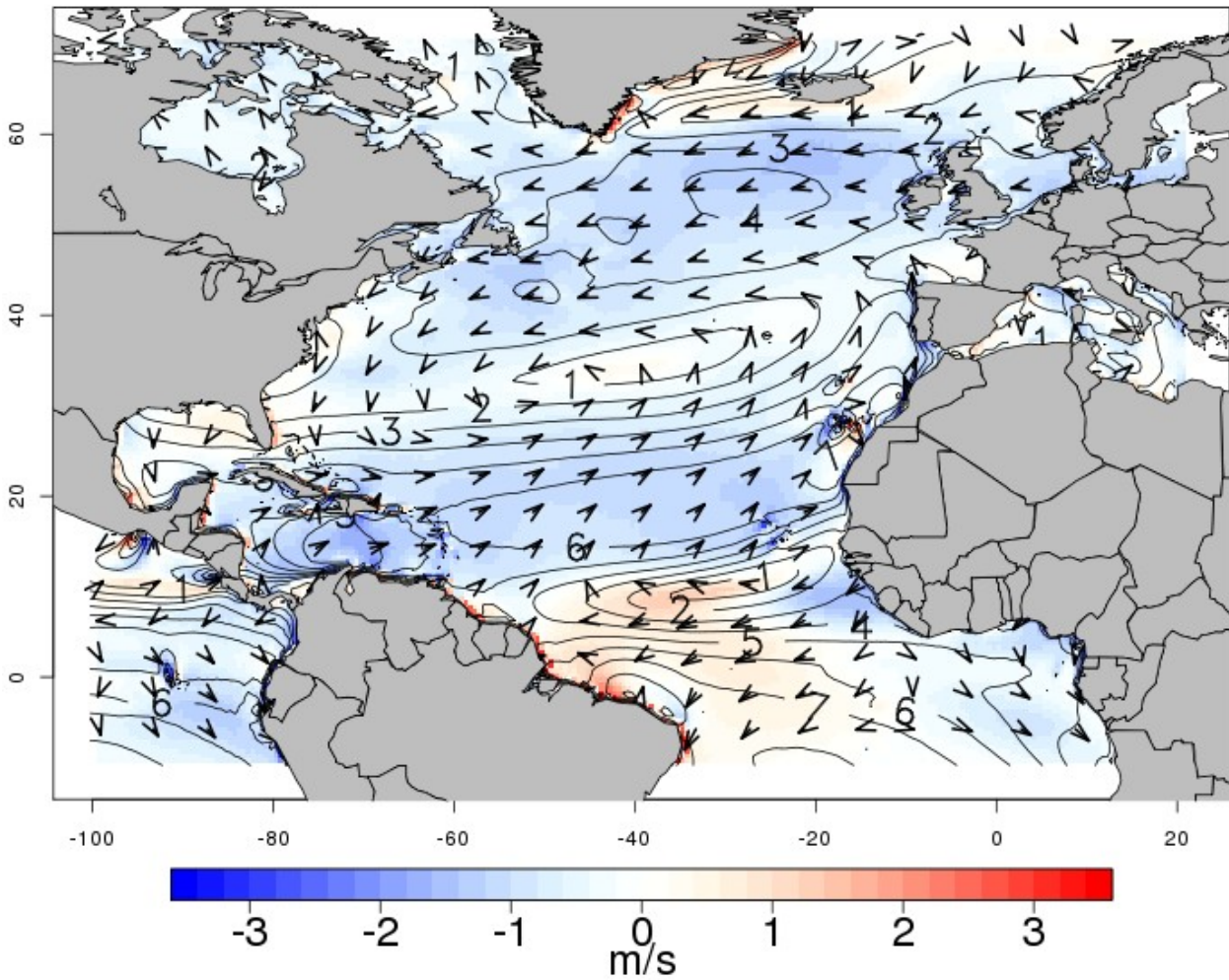
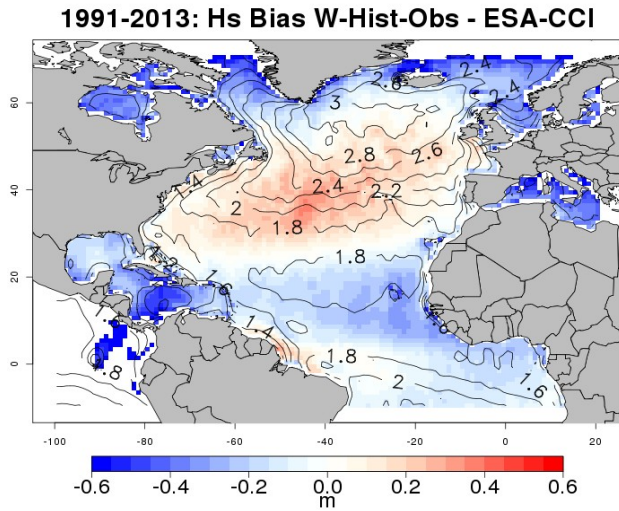


Fig. S2. Differences in the mean present-climate (1984-2013) hurricane-season surface winds (arrows) and wind speed U_{10} (shading) between Hist-Obs and ERA5. ERA5 values for U_{10} are overlaid as black contours. The data have been interpolated onto a 0.5° grid, and are masked over land. The arrows are for the difference in wind vectors. Units are $\text{m}\cdot\text{s}^{-1}$.

1039

a)



b)

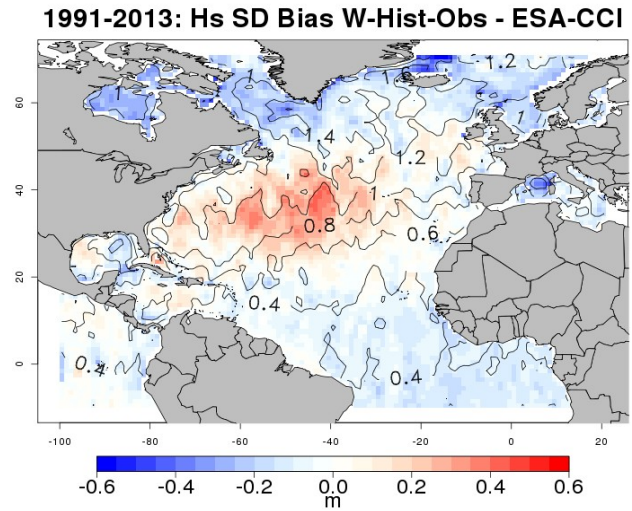


Fig. S3. Differences in the a) mean and b) standard deviation of 1991-2013 ASO significant wave height H_s (m) between MFWAM05 W-Hist-Obs and ESA Sea State CCI (shading), with ESA Sea State CCI values overlaid as black contours. The MFWAM05 data have been interpolated onto a 1° grid. Differences exceeding ± 0.6 m are masked in white.

1040

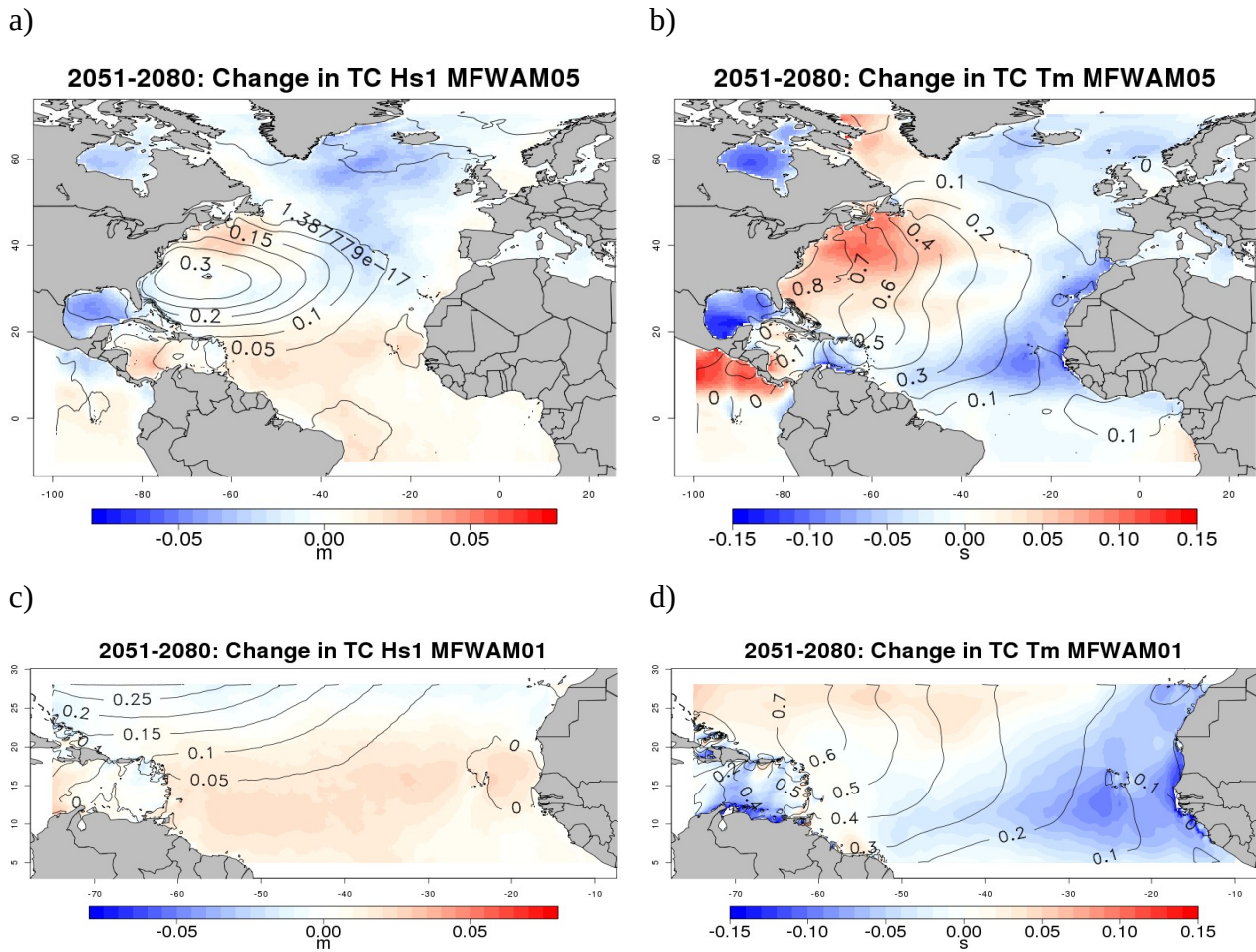


Fig. S4. Same as Fig. 9ac, except for (a,c) significant height of primary swell H_{s1} (m) and (b,d) mean wave period T_m (s).

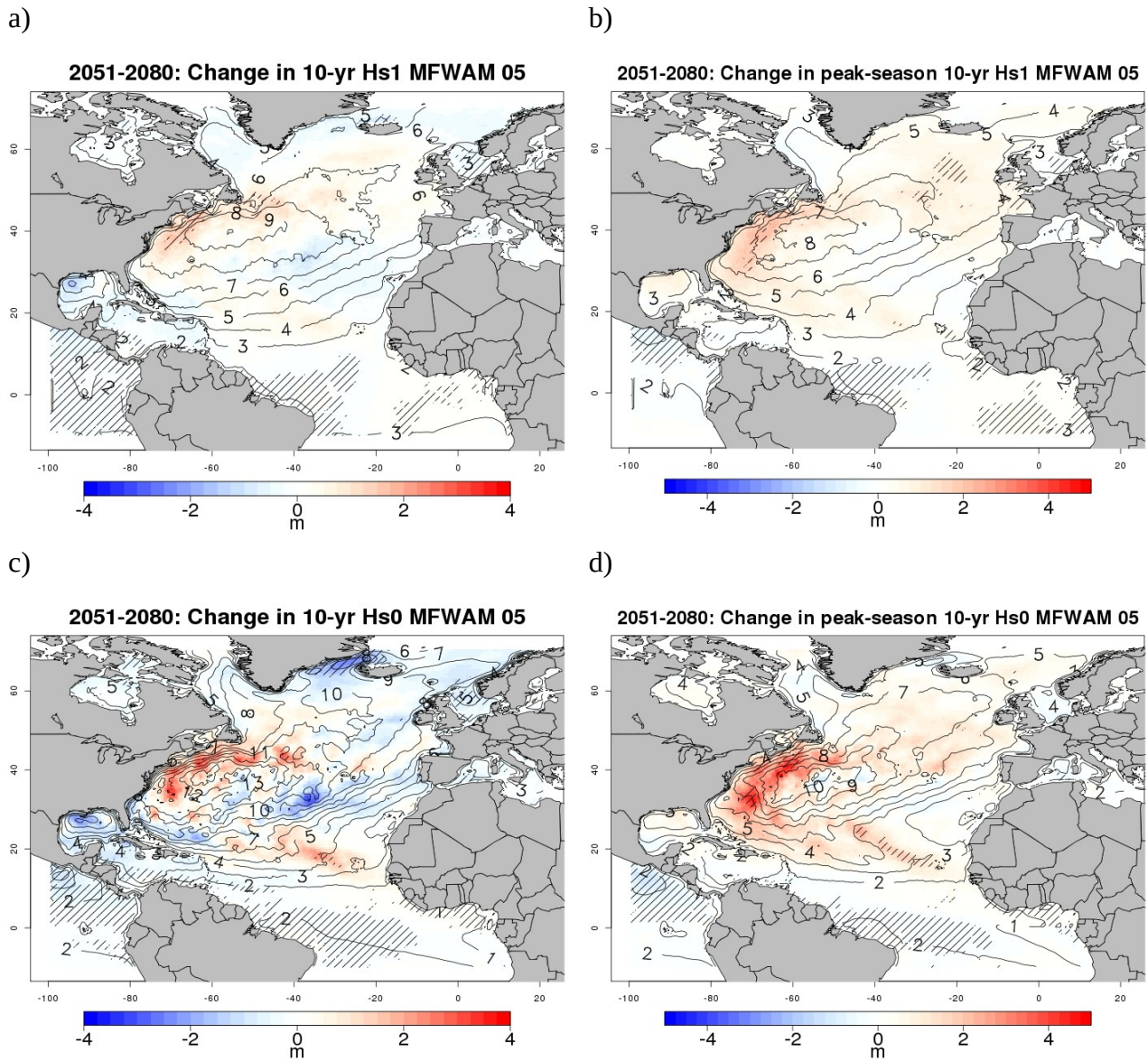


Fig. S5. Same as Fig. 10ab, except for significant height of (a,b) primary swell H_{s1} and (c,d) wind waves H_{s0} (m).

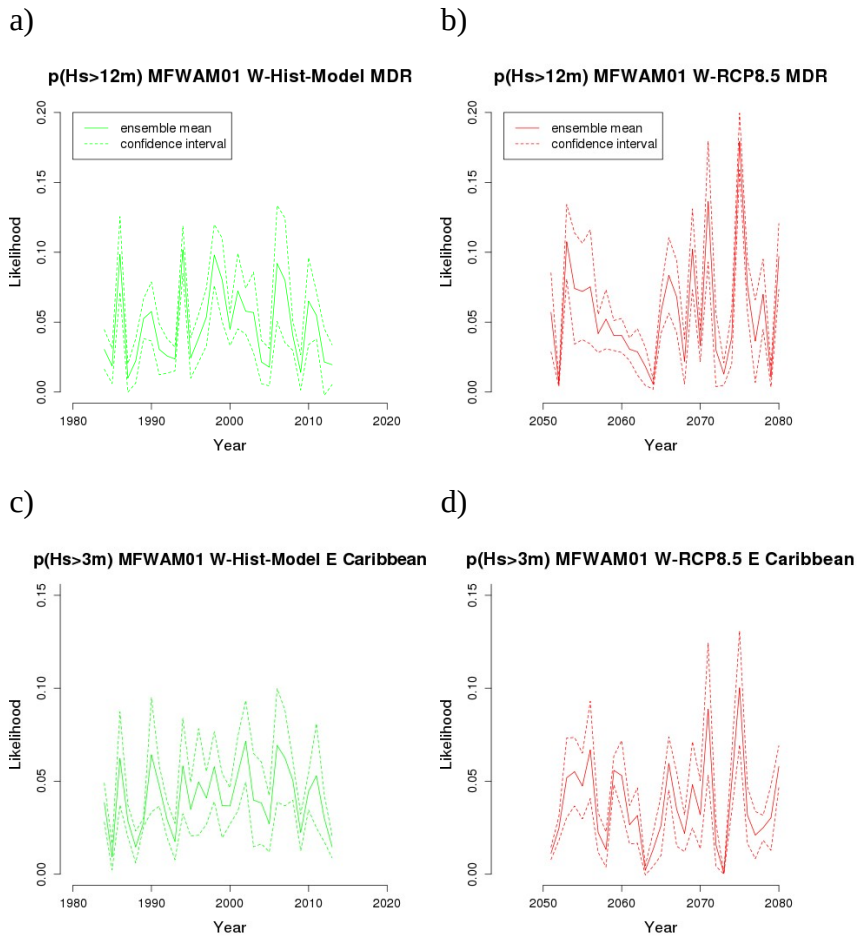
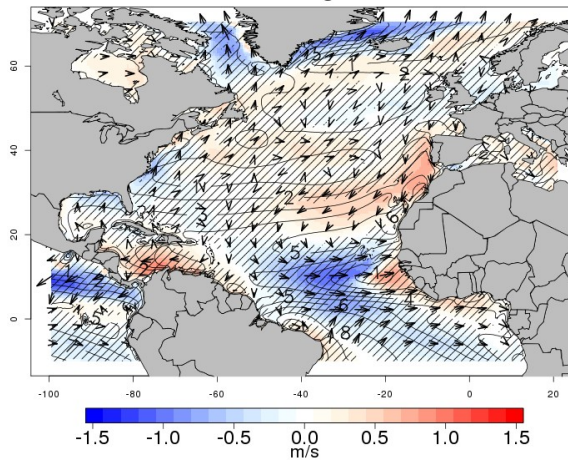


Fig. S6. (a,b) same as Fig. 11cd and (c,d) same as Fig. 11ef, except from MFWAM01.

1045

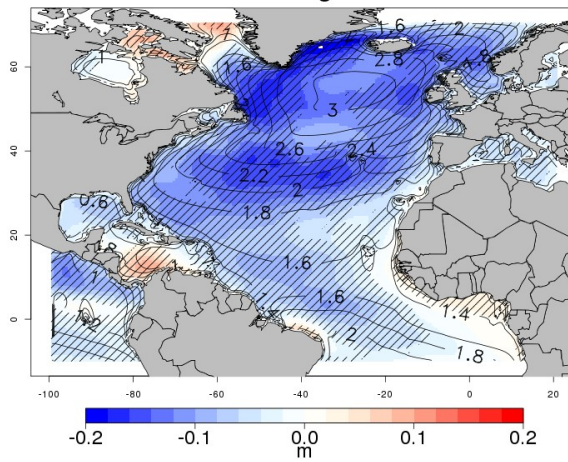
a)

2051-2080: ASO change in U10 ARPEGE



b)

2051-2080: ASO change in Hs MFWAM05



c)

2051-2080: ASO change in Tm MFWAM05

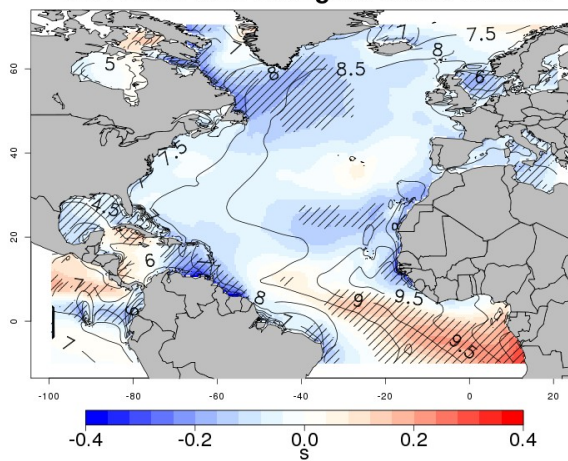


Fig. S7. Same as Fig. 5, except averaged over ASO.

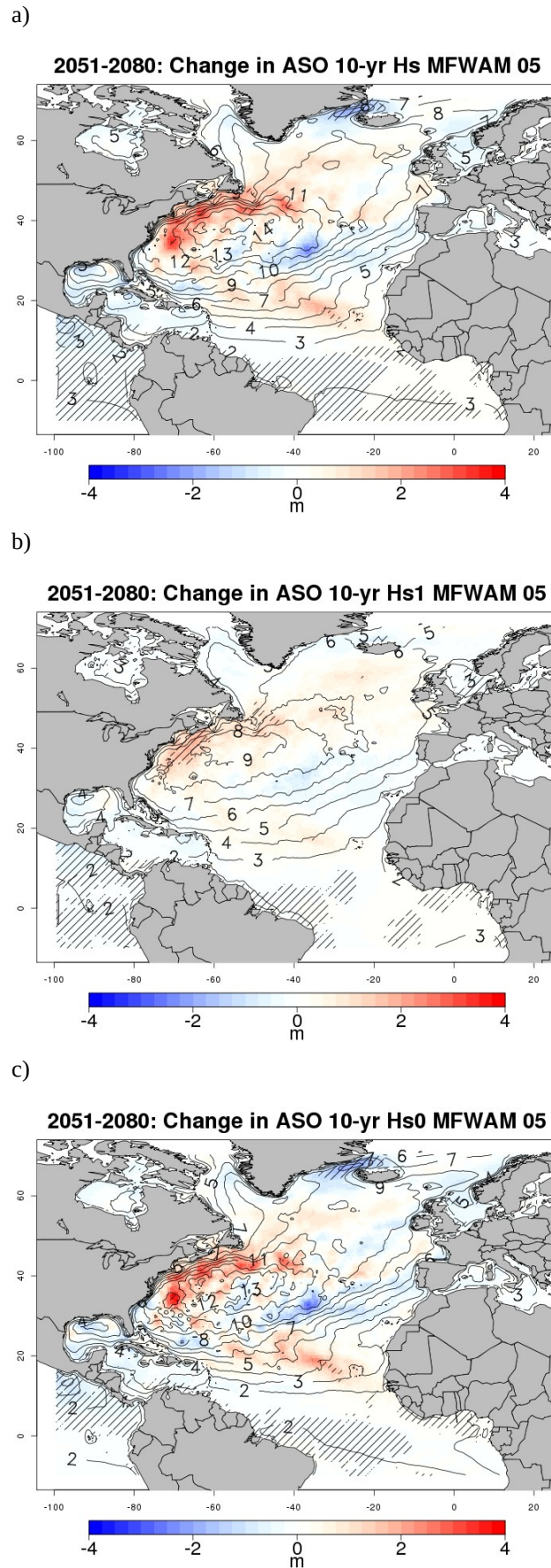


Fig. S8. (a), (b), (c) same as Fig. 10a, S5a, S5c, respectively, except over ASO.

